An Experimental Investigation of the Fluid Dynamic Aspects of a Bileaflet Mechanical Heart Valve

By

Juan Mejia

B.S., Florida Institute of Technology, 2004

A Thesis Submitted in Partial Fulfillment of the Requirements for the Degree of
Master of Applied Science
in the Department of Mechanical Engineering

An Experimental Investigation of the Fluid Dynamic Aspects of a Bileaflet Mechanical Heart Valve

By

Juan Mejia

B.S., Florida Institute of Technology, 2004

We accept this thesis as conforming
to the required standard

Peter Oshkai, Assistant Professor (Mechanical Engineering)

Edward Park, Assistant Professor (Mechanical Engineering)

Afzal Suleman, Professor and Associate Dean of Research (Mechanical Engineering)

Lawrence Scotten, External Examiner (Vivitro Systems Inc.)

Supervisor: Dr. Peter Oshkai

Abstract

Turbulent flow downstream of a bileaflet mechanical heart valve is investigated using digital particle image velocimetry. Evolution of flow structures during the systole and diastole phases of a typical cardiac cycle is characterized by obtaining global flow velocity measurements in multiple cross-sections of the flow field. Instantaneous and time-averaged patterns of flow velocity, vorticity, and streamline topology are used to illustrate the interaction between the unsteady vortices that results in elevation of shear stress levels. This image-based approach can potentially lead to development of methods of control of platelet activation and provides insight into the underlying flow physics.

Examiners:

Peter Oshkai, Assistant Professor (Mechanical Engineering)

Edward Park, Assistant Professor (Mechanical Engineering)

Afzal Suleman, Professor and Associate Dean of Research (Mechanical Engineering)

Lawrence Scotten, External Examiner (Vivitro Systems Inc.)

Table of Contents

Acknowledgments

This work would have never been possible without the help of my friends, family, and colleagues. I would like to thank all and every one of them for their contribution to this project.

In particular, my family, for giving me the means to arrive where I am today. Flo, for keeping my life outside of school in one piece, and Jeff Wishart for his valuable editorial input.

Last but certainly not least, to my supervisor Dr. Peter Oshkai for his advice, guidance, knowledge, and uncountable hours of support.

Dedication

A mis abuelos, mi hermana, y sobre todo a mis padres.

List of Figures

Chapter 1 Introduction

1.1 Native heart valve function, anatomy, and types of valve failure

In the fourth century B.C., the Greek philosopher Aristotle identified the heart as the most important organ of the human body. Since then, the heart has been the subject of studies in virtually every field. Despite this attention, ischemic attacks are currently the leading cause of death worldwide, and heart valve diseases remain among the most common types of heart disease. In fact, today, over 175,000 prosthetic heart valves are implanted in the US alone, Johansen [1]. It is therefore apparent that additional research directed at the elucidation of the causes of heart disease and methods for mitigation and prevention is required. A thorough account of both native and prosthetic heart valve function and malfunction is given by Yoganathan *et al.* [2]. Only a summary of the most relevant features in the context of this thesis will be presented here.

A human heart is a pump with four chambers and four valves, all of which serve to circulate blood throughout the body. Under normal conditions, an average heart pumps blood at a rate of 5.25 liters per minute, and beats approximately 2.5 billion times throughout the course of a lifetime. The valves located in the right-hand side of the heart are the pulmonic and tricuspid valves, while the mitral and aortic valves are located in the left-hand side of the heart, as shown in Figure 1.1-1. In general, the valves on the left heart are the most commonly affected by disease, and among them, the aortic valve is subject to the largest loads, Yoganathan *et al.* [2]. The present study focuses on the study of a valve in the aortic position.

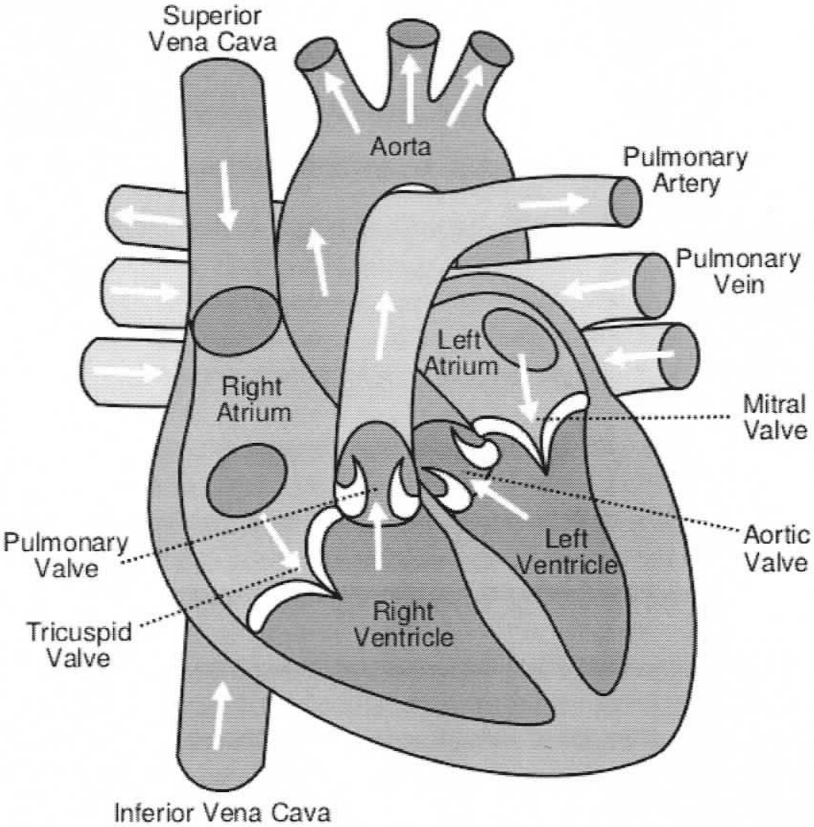

Figure 1.1-1. Diagram of the heart with complete set of valves and arteries
***source*: www.nationmaster.com, June 5 2005.**

The aortic valve, which separates the aorta from the left ventricle, is composed of three leaflets attached to a connective tissue sleeve. The first 200-300ms of the cardiac cycle are defined as the *systolic* phase, and the last 500ms of the cardiac cycle are defined as the *diastolic* phase. At the beginning of systole, the left ventricle contracts and forces blood into the aorta, opening the aortic valve. Approximately 10ms after the beginning of systole the leaflets have fully opened and the flow has reached its peak velocity of 1.35 m/s. During the rest of the systolic phase the flow through the aortic valve decelerates and the leaflets close gradually until they reach the fully closed position before diastole begins. The aortic valve remains closed throughout diastole and it is subject to pressures as high as 100mmHg, Yoganathan *et al.* [2].

When considering a single heart valve, the cardiac cycle can be fully represented by four phases: the opening phase, the fully open phase, the closing phase, and the fully closed phase. Each phase exhibits unique fluid phenomena. A brief but representative description of the fluid dynamics associated with each phase of a native aortic heart valve is given by Yoganathan *et al.* [2]:

> "During systole, vortices develop in all three sinuses behind the leaflets of the aortic valve. These vortices help to close the aortic valve quickly so that an efficient and fast closure is obtained. The closing volume, or backflow during closure, has been estimated to be less than 5% of the forward flow, Bellhouse and Bellhouse [3]. In healthy individuals, blood flows through the aortic valve at the beginning of systole owing to the transvalvular pressure and rapidly accelerates to its peak value of 1.35 ± 0.35m/s, Rossvoll et al. [4]… At the end of systole, there is a short period of reverse flow that can be measured with Doppler ultrasound. This reverse flow is probably due to either a small closing volume of the velocity of the valve leaflets as they move toward their closed position. The velocity profile orifice is almost flat, with the flow skewed slightly toward the septal wall, Kilner et al. [5]. Highly skewed velocity profiles and corresponding helical flow patterns have been observed in the human aortic arch…"

Heart valve failure can be broadly grouped into two main categories. A valve passage is said to be *stenotic* if the affected valve narrows, which increases resistance to blood flow. On the other hand, excessive regurgitation caused by a valve that does not close properly, also referred to as an *insufficient* valve, decreases cardiac output and forces the heart to work harder to supply the organs with the same amount of blood. To remedy either of these conditions, implanting prosthetic heart valves, either mechanical or biological, is currently used as a surgical treatment for heart valve disease. Contemporary research continues in an ongoing attempt to improve the state-of-the-art technology.

1.2 Development of prosthetic heart valves

The first heart valve was implanted in 1952. However, valve replacement was not considered to be a successful procedure until the 1960's, Roberts [6]. Since then, prosthetic heart valves of various types, including the caged ball, tilting disk, and bileaflet, as well as various biological valves, have been developed.

In 1951, Dr. Charles Hufnagel introduced the first mechanical heart valve to be used in clinical applications. The design of the Hufnagel ball valve consisted of a methacrylate ball contained in a methacrylate tube. Prior to 1968, several modifications to the original ball valve design were used clinically with various degrees of success. Although durable, the design of ball valves requires more work from the heart muscle to account for the change in direction necessary for the blood to clear the ball, DeWall et al. [7].

An alternative type of valve, the disc valve, was introduced in 1962. The first valve of this type was the Barnard-Goosen valve, which consisted of a modified disc with attached restraining projections. A year later, the Lillehei-Cruz-Kaster tilting disc valve was introduced. In this design, major and minor orifices are divided by a tilting disk, with high-velocity regions flowing from both the major and minor orifices.

The major complications related to early ball and disc valves were related to material erosion or fatigue, DeWall et al. [7]. The problem was partially resolved by the introduction, in 1969, of a pyrolitic carbon called *Pyrolyte*. Although hard to manufacture and machine, Pyrolyte has exceptional biocompatibility and is extremely hard. However, ball and disc valves are multi-component mechanisms, and not all components can be manufactured out of Pyrolyte. Therefore, material erosion remained an issue for early valves of this type, DeWall et al. [7].

In 1977, the first bileaflet mechanical heart valve was implanted by Dr. Demetre Nicoloff, DeWall et al. [7]. Bileaflet valves have two semicircular leaflets that divide the area available for forward flow into three regions: two lateral and one central orifice. This design allowed for the entire valve, with the exception of sewing ring, to be made out of Pyrolyte, DeWall et al. [7]. Today, the bileaflet mechanical heart valve is the most commonly implanted valve in the world.

Meanwhile, since the mid-1970's, biological valves have been used as an alternative to mechanical heart valves. Although originally considered to be the ideal solution by some valve manufacturers, biological valves were found to be less durable than their mechanical counterparts. Even today, the three biggest valve manufacturers, namely Medtronic, St. Jude and Baxter-Edwards, are still focusing their efforts on improving the long-term durability of biological valves, Vesely [8].

1.3 Mechanical vs. Biological Prosthetic Heart Valves

Prosthetic heart valves can be broadly categorized into biological or mechanical types. Both types of heart valves have associated advantages and disadvantages. Presently, it is not clear whether one type of valves is significantly better. In general, prosthetic heart valve design requirements can be briefly summarized as structural durability, biocompatibility, and compliance with physiological flows.

Compared to mechanical heart valves (MHVs), biological valves do not require the use of blood thinners (anticoagulant drugs) to be administered to the patient, making them an attractive alternative. However, earlier biological valves exhibit relatively large pressure drops, deteriorate faster, and undergo rapid calcification, Woo *et al.* [9]. Overall, biological heart valves comply better with physiological flows but lack durability.

On the other hand, mechanical heart valves are generally considered to have long term durability, but do not comply well with physiological flows, thus increasing the risk of thromboembolisms. Therefore, a comprehensive study encompassing both biological and mechanical heart valves should be undertaken. However, due to the importance of MHVs to the medical community, the focus of the present study is on the fluid dynamics of a bileaflet MHV.

1.4 Mechanical prosthetic heart valve background

Mechanical Heart Valves (MHVs) are considered relatively durable but are strongly associated with *thrombogenicitys*, which can cause thromboembolisms, ischemic attacks and stroke, Yin *et al.* [10]. A thromboembolism can cause occlusion of a blood vessel due to a blood clot. Studies have shown that unphisiological stress on *platelets*, which are ellipsoid discs 2-4μm in diameter that flow in the blood stream, are closely linked to the occurrence of thromboembolisms. Platelet activation is the main mechanism that causes formation of *thrombi*, commonly known as blood clots, Snyder *et al.* [11]. Further studies found a strong link between platelet activation and high levels of shear stress in the blood flow. It is now well accepted that excessive exposure to shear stress causes platelet activation, Hellums [12].

Therefore, it has been suggested that thrombi are caused by flow phenomena that are not characteristic of physiological conditions, Bluestein *et al.* [13]. The flow phenomena that receive the most attention in this respect include: jet-like flow regions, regions of elevated shear stress, flow separation regions, shed vortices, and turbulence characteristics, Yin *et al.* [10]. Despite the recent advances in the field, thromboembolisms occur in approximately 3% of all replacement operations involving MHVs, Edmunds *et al.* [14].

Existence of many different types of MHVs requires the definition of a comparison parameter. The effective orifice area (EOA) is an index that represents how well a valve design utilizes the area in which the valve is mounted. EOA is defined by Yoganathan et al. [15] as follows:

$$EOA(cm^2) = \frac{Q_{rms}}{5.16\sqrt{\Delta p}}, \tag{1}$$

where Q_{rms} is the root mean square systolic/diastolic volumetric flow rate (cm^3/s) and Δp is the mean systolic/diastolic pressure drop (mm Hg). The EOA is related to the total fluid jet core area. It depends on the design features and size of the valve, and some studies normalize the EOA by the valve sewing ring area. The resulting non-dimensional parameter is the performance index (PI) of a valve. A large variety of valves with their corresponding EOAs and PIs are listed by Yoganathan *et al.* [2].

1.5 Review of literature

A number of experimental and numerical studies have been undertaken in order to address issues associated with both biological and mechanical heart valves.

Nevertheless, there still is an incomplete understanding of the fundamentals governing flow phenomena, associated with heart valves.

1.5.1 Experimental Studies

Significant effort has been devoted to the development of realistic laboratory models capable of simulating fluid mechanic characteristics of the human heart while allowing optical access for the purpose of flow visualization. The complexity of the biological system calls for a flow chambers that not only preserves geometric similarity but also models viscoelastic components, and the pressures of the pumping cycle. Anatomically correct mock-ups of the aorta have been successfully manufactured and investigated. Scotten and Walker [16] developed a model of the left heart, which included a viscoelastic model ventricle, compliance elements in the aortic root, systemic compliance, and peripheral resistance. It allowed the simulation of an arbitrary cardiac cycle and provided optical access to valves in both the aortic and the mitral positions. Several studies have been conducted using this setup, including the development of a new technique to measure the projected dynamic area of prosthetic heart valves, Scotten and Walker [16]. The study found current mechanical valves to open more slowly than their biological counterparts during systole and diastole, to have high variations in terms of dynamic open area from cycle to cycle, to close more abruptly than biological valves, and to rebound after the first contact with the valve housing during closure.

With the development of particle image velocimetry (refer to section 2.1 for a detailed description of particle image velocimetry), many research efforts applied this full-field non-invasive flow visualization technique to study flow structures associated with prosthetic heart valves. Marassi et al. [17] developed an artificial heart valve test bench specifically designed to employ particle image velocimetry (PIV). Test benches for digital PIV and stereo PIV were developed. Both designs consisted of a valve mounted in a Plexiglas channel. In both cases, the channel was surrounded with a Plexiglas chamber to minimize optical distortions. This design delivered high versatility in changing and controlling the flow parameters and good optical access for visualization experiments.

An alternative, albeit a less popular approach to manufacturing an anatomically correct mock-up is performing *in vivo* experiments. Kleine et al. [18] studied the effects of orientation of both monoleaflet and bileaflet valves implanted in a pig's heart. It was found that valve rotation, performed by way of fishing line attached to the valve and manipulated by hand, had a profound effect on the flow structure associated with the monoleaflet valve. When the large orifice, of the monoleaflet valve, was oriented in the direction of the right posterior aortic wall the aortic flow largely complied with physiologic conditions. On the other hand, the bileaflet valve produced turbulent flow in its wake at any orientation. These results implied that a correctly oriented monoleaflet valve can perform better than a bileaflet valve.

It has been suggested that among the many possible causes of thromboembolisms, vortex shedding from the leaflets of MHVs is among the most critical. The shed vortices are associated with regions of high shear stresses in the flow. Blood components, e.g. platelets, can become entrapped in these vortices for relatively long periods of time, increasing their chance of becoming activated.

Several studies have focused on the fundamental fluid dynamics of MHVs in order to provide insight into the flow phenomena. Castellini et al. [19] employed PIV techniques to obtain flow velocity measurements upstream and downstream of a bileaflet valve. A symmetric flow pattern including a large separation region behind each leaflet was observed. Furthermore, the authors observed regions of high velocity between the leaflets as well as between each leaflet and the channel walls, which represented the walls of the aorta. Vortex shedding from the trailing edge of each leaflet was also documented. Zhao and Yeo [20] investigated the flow fields corresponding to different hinge positions. The flow patterns were found to be symmetric, with separation regions present on the inner surface of the leaflets. The pulsatile flow was modeled by employing a pressure waveform corresponding to a typical cardiac cycle. In order to compensate for the limited temporal resolution of the PIV measurements, the waveform was stretched over a period of 10 seconds. Brucker et al. [21] studied the pulsatile flow through a trileaflet MHV using PIV to obtain velocity field measurements downstream of the valve. The authors observed a well-defined core flow with small wakes behind each leaflet. The trileaflet MHV was found to provide a desirable wash-out effect of the stagnant regions in the aortic sinuses, as well as a reduced impact velocity during the closing phase of the cardiac cycle.

Bluestein et al. [22] performed a study of pulsatile flow through a bileaflet MHV mounted in a non-compliant aorta model. The technique of digital particle image velocimetry (DPIV) was used to characterize the flow. The authors assumed (based on the results of Lamson et al. [23]) that no single phase of the heart cycle (i.e. opening, fully open, closing, or fully closed) contributed significantly more to the formation of thrombi than any other phase. However, a number of other investigations have focused on particular phases of the cardiac cycle. In fact, during the 1970s and 1980s, most of the studies implicitly assumed that blood damage occurs predominantly during forward peak flow through the valve. This assumption is intuitive, as the flow rate is at its maximum when the valve is fully open, but later studies have challenged the validity of this assumption. Manning et al. [24] investigated the regurgitant flow field of a bileaflet MHV using PIV under physiological pulsatile flow conditions. The authors found strong jets emerging from the two hinges, and two weaker jets originating from the regions of transition between the tightly sealed central plane and the hinge region. Maximum viscous shear stresses were found to be of the order of 20 N/m^2, which is below the shear stress traditionally associated with the onset of hemolysis. However, Meyer et al. [25] used Laser Doppler Velocimetry (LDV) to measure the Reynolds stress associated with the regurgitant flow of three different mechanical heart valves and found that relatively high turbulent stress levels (maximum of 360 N/m^2) were possible for each of the three valve designs. At present, there is no clear consensus in the research community as to whether a certain phase of the cardiac cycle can single-handedly cause thrombus formation, or even which phase contributes the most to the problem of thrombogenicity.

1.5.2 Numerical Studies

Numerical methods play a fundamental role in the research of fluid dynamics. For example, numerical simulations can provide detailed three-dimensional, time-resolved information about a flow. Hence, an integrated approach involving both experimental and numerical techniques is often required to fully characterize a fluid flow problem.

As thrombogenicity is closely linked to platelet activation a number of studies have focused on the effect of prosthetic heart valves on platelet activation. If a platelet reaches a certain threshold of cumulative exposure to high shear stress, it becomes activated. The platelet activation state (PAS) was studied for monoleaflet and bileaftlet valves by Yin *et al.* [10]. The authors considered both shear stress magnitude and time of exposure of a given platelet to the elevated shear stress to determine the PAS. In order to numerically determine the amount of activated platelets, tracers were introduced to the calculated flow. The exposure of a tracer to shear stresses over a period of time was then evaluated. Monoleaflet valves were found to cause less PAS compared to bileaflet MHVs. Furthermore, the results showed that virtually no PAS existed in a control case when the valve was removed from the flow field.

Bluestein et al. [22] identified vortex shedding as a possible mechanism for the activation of platelets: "The shed vortices also provide the flow conditions that promote the formation of larger platelet aggregates… Following activation, platelets will release their granule constituents and provide positive feedback reactions of coagulation. Platelet aggregates will increase the efficiency of the reaction, eventually resulting in the formation of free emboli."

A numerical simulation of the closing phase of a bileaflet MHV was performed by Lai et al. [26]. It was found that the negative pressure quickly develops on the atrial side of a valve leaflet tip and on the valve housing. The pressure reaches its lowest value just before the valve fully closes. It was determined that the low local pressure is caused by the dynamics of the shed vortices. Furthermore, it was shown that the clearance gap and tip angle of the valve does not influence the associated fluid dynamics significantly. On the other hand, the speed at which the leaflet closes can have a dramatic effect in terms of the local pressure decrease. In fact, the study showed that reducing the leaflet velocity in the last four degrees of its motion by a factor of three leads to a reduction of both the maximum positive and negative pressures by more than 50%. This numerical simulation did not take into account coupling between the wakes caused by the two leaflets that was observed by Hirt et al. [27].

Recently, fluid-structure interaction phenomena have been incorporated in several numerical models. Cheng et al. [28] developed a three-dimensional model to study the flow dynamics associated with a MHV. Vortical structures were reported in the region between the valve's leaflets and the valve housing, and large wall shear stresses were calculated at the leaflet's edge during the impact-rebound phase of the cardiac cycle.

Ellis et al. [29] performed Laser Doppler Velocimetry (LDV) measurements in the hinge region of a Medtronic Parallel bileaflet MHV. Peak velocities of 3m/s in the hinge region were reported during the back flow phase of the cardiac cycle. Further, "the high turbulent stresses near the top of the inflow channel, combined with a persistent vortex, implicate the inflow channel of the hinge as a likely region of thrombus formation." In a similar study of a St. Jude bileaflet MHV, Ellis et al. [30]

reported peak velocities in the hinge region of 2.1m/s. The LDV measurements performed on the St. Jude valve showed a reduction of 56% in peak Reynolds stress levels in comparison to the Medtronic Parallel valve.

1.6 Research objectives

The present work is a part of a larger effort seeking a better understanding of the fluid dynamics associated with mechanical heart valves that could help in improving the design of future valves. It focuses on the bileaflet mechanical heart valve. The MHV's popularity is largely due to its durability, but compared to biological valves, bileaflet MHVs require substantial improvements in terms of their fluid dynamic performance, which relates to thrombogenicity. Thus, with the present study an attempt is made to elucidate many of the flow features that are associated with a bileaflet MHV.

Out of the four phases of the cardiac cycle, only the fully open and the fully closed valve flow phases will be considered here. An investigation of the bileaflet valve under steady conditions is the first logical step in an ongoing effort to fully characterize the fluid dynamics of bileaflet MHVs. Nevertheless, it is clearly necessary to undertake a time-dependent investigation of the entire cardiac cycle. Therefore, in an effort to provide solid ground for a continuation of this work a pulsatile flow loop has been designed.

In the past, the phase of the cardiac cycle that corresponds to the fully open aortic valve (peak systole) has been subject to numerous investigations. However, the development of particle image velocimetry (refer to section 2.1 for a brief history of particle image velocimetry) has provided a valuable tool that could potentially shed light on many of the issues that remain unanswered about this phase of the cardiac cycle. Nonetheless, previous works are useful as they provide the opportunity to compare and validate some of the results presented here.

On the other hand, the phase of the cardiac cycle that corresponds to the fully closed aortic valve (peak diastole) has received considerably less attention. Only recently has it been suggested that leakage through the closed valve can potentially cause damage to blood cells.

In this study the same amount of attention is given to the fully open and fully closed phases of the valve's cycle. An attempt is made to characterize the highly three-dimensional structure of the flow downstream of a bileaflet MHV by resolving two-dimensional velocity fields at different vertical and horizontal locations downstream of both the open and closed valve (refer to section 2.3 for description of the modeling of the phases of the cardiac cycle). Using this approach the flow structure at different locations downstream of the bileaflet MHV can be characterized. It is also possible to determine flow features that could potentially contribute to the activation of platelets.

Chapter 2 Experimental System and Techniques

The experiments for the current study focused on modeling of the fully open and fully closed phases of the cardiac cycle. A steady-state investigation of the bileaflet valve is done here as a first logical step in an ongoing effort to fully characterize the fluid dynamics of bileaflet MHVs.

2.1 Particle image velocimetry

Particle image velocimetry (PIV) is a non-intrusive optical flow diagnostic technique. The underlying principle of PIV is based on the lack of significant interaction between an optically homogeneous fluid and a source of incident light. Thus, in PIV the fluid motion is made visible by adding small tracer particles that scatter the incident light. From the position of these tracer particles at two consecutive instants, with a known time delay, the velocity of the fluid can be inferred.

2.1.1 Brief history of particle image velocimetry

Seeding a flow, with smoke, dies, or particles, as a way to accomplish flow visualization is a simple and commonplace technique. Hence, the underlying principles of particle image velocimetry are not new. However, the development of an accurate and reliable full-field technique was a long and complicated task. A representative history of PIV is given by Adrian [31].

Briefly, the initial groundwork for particle image analysis was given by Adrian [32] in 1984 and almost a decade later the theory was generalized to include multiple-exposure recordings, Adrian [33]. Later, digital cameras, computers, and double-pulsed lasers were introduced to arrive at the off-the-shelf technology that is commercially available today. Since the beginning of the new millennia "the focus…

has been on developing accurate, robust means of measuring the image displacement from the image field. It appears that we are closing in on algorithms that are near optimum, and that relatively little can be expected in terms of future improvements in performance." Adrian [31]

Not only is the technology associated with PIV mature, the technique has been thoroughly validated. An example of such a validation is given by Westerweel [34]. Therefore, since the study of flow through a bileaflet mechanical heart valve requires a full-field non-intrusive technique, particle image velocimetry is an ideal candidate for the purposes of this investigation.

2.1.2 Fundamentals of particle image velocimetry

In particle image velocimetry (PIV), the fluid motion is made visible by means of adding tracer particles to the flow. To avoid sub-pixel displacement, particles added to liquids, as a rule of thumb, should be on the order of 1-10μm and need to be neutrally buoyant (i.e. have the same density as the fluid they are seeding). Further, the flow must be homogeneously seeded such that any flow structure can not be visible until the velocity field is calculated. Finally, the seeding density must match the smallest length scale of the spatial variation in the flow field under investigation, Westerweel [34].

The particles are illuminated by a sheet of light that is pulsed, usually provided by a double-pulsed laser. The particles then scatter the light into a recording medium positioned perpendicular to the laser sheet. The recording medium, normally a photographic lens, must be located such that its in-focus object plane coincides with the location of the laser sheet. In order to maximize signal to noise ratio the intensity of the laser must ensure high-contrast between the background and the particles. Generally, higher intensity levels are desirable as long as unwanted reflections do not decrease visibility.

For flow fields with large velocity magnitudes perpendicular to the laser sheet the thickness of the sheet becomes a parameter of extreme importance. As a rule of thumb, the sheet should be thick enough such that particles take four times the time delay between the two laser pulses to cross the entire thickness of the laser sheet. Mathematically,

$$x = 4\bar{U}_r dt \, , \tag{2}$$

where x is the laser sheet thickness, $\bar{U}_r$ is the average particle velocity perpendicular to the laser sheet, and dt is the time delay between the two exposures. A plot of this expression for five different time delays is shown in Figure 2.1-1. Using a laser sheet with correct thickness ensures the vast majority of particles captured during the first laser pulse will remain in the field of view during the second laser pulse, thus minimizing erroneous measurements.

The images are then digitized, transferred, and analyzed, which is done, thanks to the recent advances in computer technology, by a comprehensive software package. The analysis, or interrogation, of images is the most time consuming and complicated step in the process. It is also the most important step as it largely determines the accuracy, reliability, and spatial resolution of the measurements, Adrian [33].

In general, there are two basic approaches for the determination of particle displacement, each corresponding to a different type of interrogation algorithm. The first, *autocorrelation*, takes an input of a single image with multiple exposures. Alternatively, *cross-correlation* requires two consecutive images each exposed once. In either case, a velocity field, referred to herein as a *frame*, can be generated from the interrogation of the particle image(s).

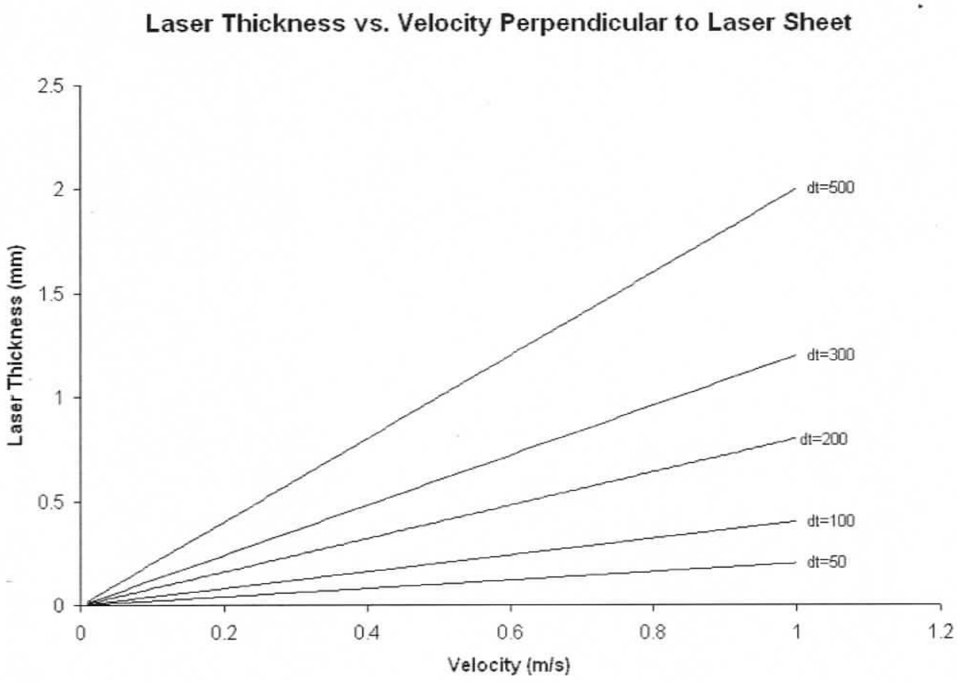

Figure 2.1-1. Necessary laser thickness for a range laser pulse time delay as a function of velocity perpendicular to the laser sheet.

Autocorrelation only requires one image recording per frame and thus allows for a higher temporal resolution. However, since each image contains multiple recordings of the same particle an issue with directional ambiguity arises. In contrast, the use of a cross-correlation algorithm does not present the same problem, although it is limited in temporal resolution by the recording medium, and therefore can be used to investigate a larger range of flows. Consequently, most preassembled commercial PIV packages today implement cross-correlation algorithms as a default, although some provide the user with a choice between the two methods. A comprehensive comparison between autocorrelation and cross-correlation is given by Westerweel [34], and a detailed analysis of the errors associated with both types of algorithms is given by Forliti et al. [35]. The cross-correlation algorithm was chosen for the present study because a review of the literature suggested the existence of large recirculation regions downstream of the bileaflet MHV, which would present directional ambiguity issues in the case of an autocorrelation approach. Therefore, for the scope of this work, only a brief description of cross-correlation and its associated analysis is presented.

The commercial software used in the fluid dynamics lab at the University of Victoria is Davis 6.2 dustributed by LaVision GmbH of Germany. This software implements the following correlation function:

$$C(x,y) = \sum_{x=0,y=0}^{x<n,y<n} I_1(x,y)\cdot I_2(x+dx,y+dy), -\frac{n}{2} < dx,dy < \frac{n}{2}, \qquad (3)$$

where "I_1 and I_2 are the image intensity of the first and second interrogation window and the 2D-array C gives the correlation strength for all integer displacements (dx,dy) between the two interrogation windows, while n is the size of the interrogation window and usually also the size of the correlation plane, i.e. $\pm n/2$ is the maximum displacement computed." LaVision [36]. For this particular work, the correlation function was used in conjunction with an adaptive multi-pass sequence. An *adaptive multi-pass* simply means the correlation peak is calculated i number of times with decreasing interrogation window size. On the first pass the correlation peak, which corresponds to the most frequent particle displacement within the window, is calculated. This correlation peak is then translated into a reference vector, which is then used as the most probable shift for the following smaller interrogation window. This process is repeated i times until the final window size is reached. This method allows for improved spatial resolution that would otherwise not be possible. However, it significantly increases processing time and the use of computer resources.

Once a velocity field has been obtained, a significant amount of information can be extracted from it. For the purpose of this work, the following parameters were calculated, from the instantaneous velocity fields (for corresponding equations refer to Appendix A): vorticity, time-averaged vorticity, root-mean-square of velocity fluctuations, and Reynolds Stresses.

2.2 Experimental set-up

The complete flow loop, illustrated in Figure 2.2-1, consisted of a transparent channel, a test section, flexible tubing, a water reservoir, a pump, and a flow meter with a built-in regulator.

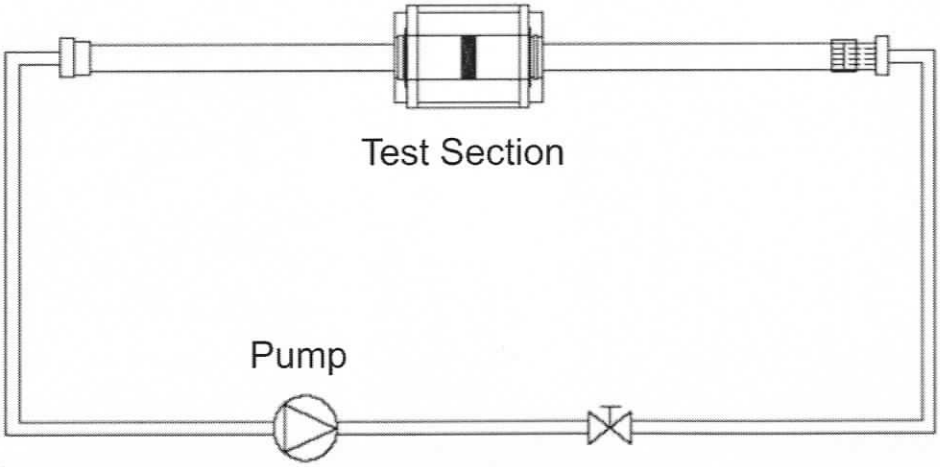

Figure 2.2-1. Complete Flow Loop.

The transparent channel is entirely constructed of Plexiglas, with a diameter of 20mm. The test section's design provides optical access to the region upstream and downstream of the heart valve. It is located 254 mm downstream of the main duct inlet. A honeycomb flow straightener is employed directly downstream of the inlet. To minimize optical distortions, a prismatic acrylic chamber filled with the working fluid surrounding the test section is employed during the experiments. A detailed schematic of the test section is provided in Figure 2.2-2.

The volume of the reservoir is $0.0247m^3$. It is necessary to periodically clean the reservoir as dust particles and other residues accumulate, contaminating the fluid.

The experiments are conducted using a Carbomedics bileaflet mechanical heart valve with an inner diameter of 20mm. This valve has an effective orifice area (EOA) of $1.66cm^2$ and a performance index (PI) of 0.48. The valve is mounted in the Plexiglas duct within the test section, as shown in Figure 2.2-2.

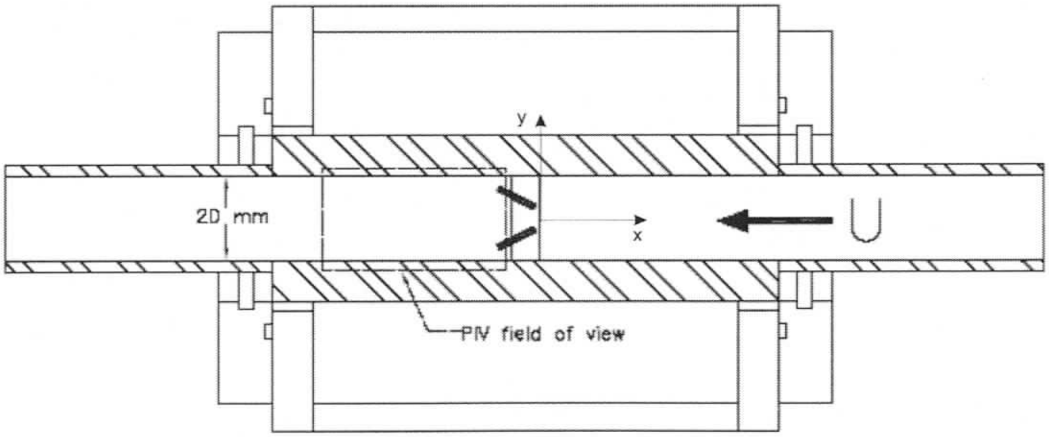

Figure 2.2-2. Close-up of test section.

Quantitative flow visualization is accomplished by employing digital particle image velocimetry (DPIV). Titanium dioxide seeding (nominal diameter of 1μm when wetted) serves as tracer particles for the experiments. This particle size was successfully applied in previous investigations by Martin [37], and each particle corresponded to approximately 1.5 pixels after image digitization. A double head Nd:Yag type IV laser (wavelength 532nm) provides illumination in the form of a laser sheet. The laser is fired twice with a known time delay. Depending on the flow velocity and the magnification factor of the camera lens, the time delay between the two pulses is chosen such that adequate displacements of the particle images on the recording medium are obtained. A high-resolution charge-coupled device (CCD) camera, capable of recording up to 4.9 cross-correlated image pairs per second, captures images of the particles, which are illuminated by the planar laser sheet. The camera is positioned perpendicular to the planar laser beam. All light, with the exception of the laser's wavelength, are filtered out by means of an optical filter mounted on the camera's lens. Both the laser and camera are electronically controlled by a dual-processor IBM-compatible computer. All electronics were provided as part of a pre-assembled commercial package by LaVision.

The images are processed on a computer yielding global instantaneous flow velocity measurements as well as maps of vorticity, streamline topology and time-averaged flow parameters. Particle displacement is inferred from a pair of consecutive images, taken with a known time delay. The recorded particle displacement is measured locally across the whole field of view of the images, scaled by the image magnification and then divided by the known laser time delay to obtain a velocity vector at each point.

For the present study, a lens with a focal length of 60 mm is used in conjunction with a 1376 x 1040 pixel CCD camera to provide a physical resolution of the velocity vector field of 4 vectors per square millimeter.

As with all free-space optics, alignment is a major issue. For this study it is necessary to align the laser sheet with both the horizontal and vertical axes. Each one of these positions requires calibration of the laser head, and alignment of the camera, the laser, and the flow channel.

As a reference, the flow channel is always aligned with the horizontal axis, as shown in Figure 2.2-3. Consequently, alignment of the laser sheet with the horizontal axis results in two-dimensional streamwise cuts of the flow field. On the other hand, alignment of the laser sheet with the vertical axis results in cross-sectional cuts of the flow field.

Laser position is recorded and measured by means of light sensitive paper (ZAP-IT Corporation laser alignment products). Once the laser sheet is fired on the light sensitive paper a permanent record of the laser's alignment, position, and thickness is obtained.

The CCD camera's optical lens must, at all times, be perpendicular to the laser sheet. Therefore, a camera aligned with the horizontal axis is needed to obtain cross-sectional cuts of the flow field, and a camera aligned with the vertical axis is needed to obtain streamwise cuts of the flow field, as shown in Figure 2.2-4. In both cases the camera is aligned by means of a spirit level.

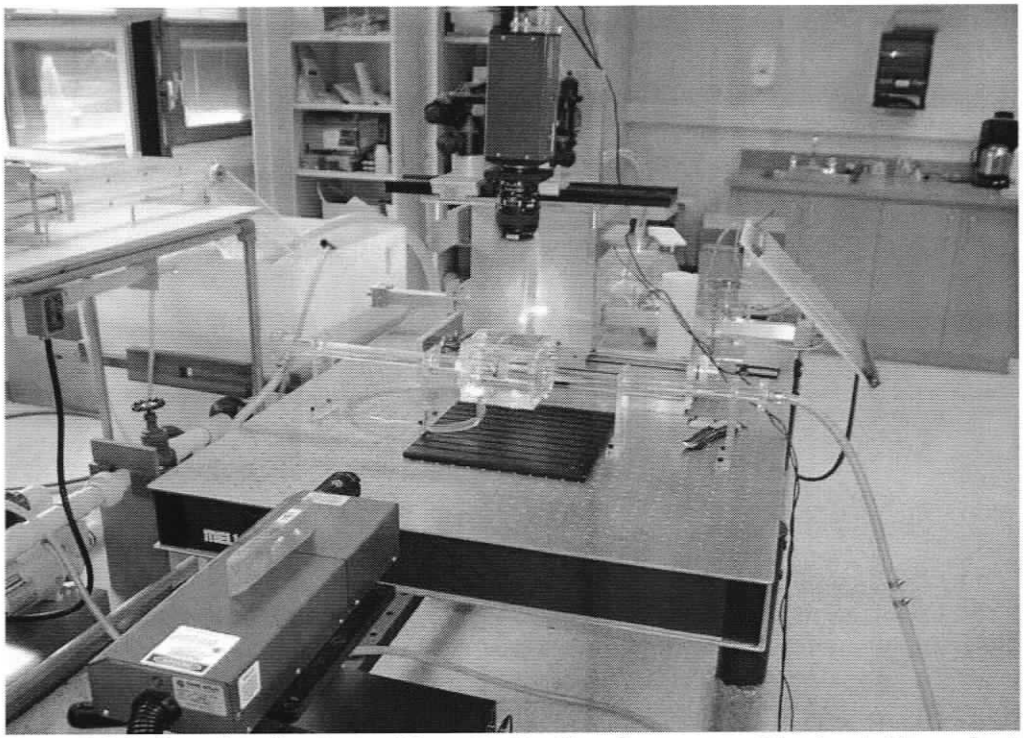

Figure 2.2-3. Complete flow loop with vertically aligned camera and horizontal laser sheet.

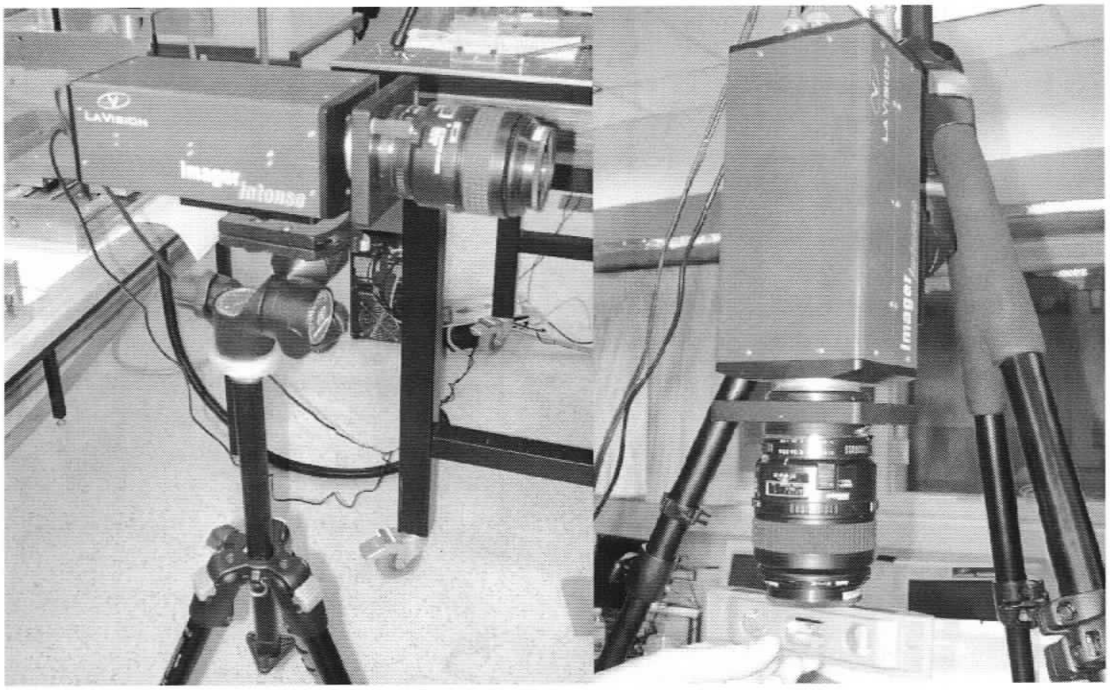

Figure 2.2-4. Horizontal (left) and vertical (right) camera set-up. For both cases cameras were aligned by means of spirit levels.

The PIV measurements are acquired at a time interval of 0.204 s, which provides spacing in time appropriate for obtaining random samples for the calculation of averaged turbulence statistics. A total of 1000 images are acquired and used in the calculation of the following time-averaged parameters: flow velocity $\underline{v}$, out-of-plane vorticity ω_z, root-mean-square values of velocity components u_{rms} and v_{rms}, and Reynolds stress correlation $\langle u'v' \rangle$.

Generally, there are two types of errors in particle image velocimetry: bias and precision errors. Bias errors are represented by erroneous correlations that result in wrong or missing vectors, herein referred to as bad vectors. Precision errors correspond to the accuracy with which the particle displacement is calculated.

A typical raw vector field is shown in Figure 2.2-5. Bad vectors, obtained due to an inappropriate cross-correlation, have not yet been removed or replaced. A total of 4576 vectors are calculated within the region of interest, and approximately 100 of those vectors are bad vectors resulting in a 2% bias error. These vectors are later removed and replaced by means of interpolation.

Further, in PIV the location of the correlation peak is directly associated with the particle displacement. By itself, calculating the cross-correlation function allows to located the peak with a precision of ±0.5 pixels. However, with the use of Gaussian curve-fitting method it is possible to increase the accuracy by approximately 20%. Thus, for an average particle displacement of 1mm the precision error is approximately 2%.

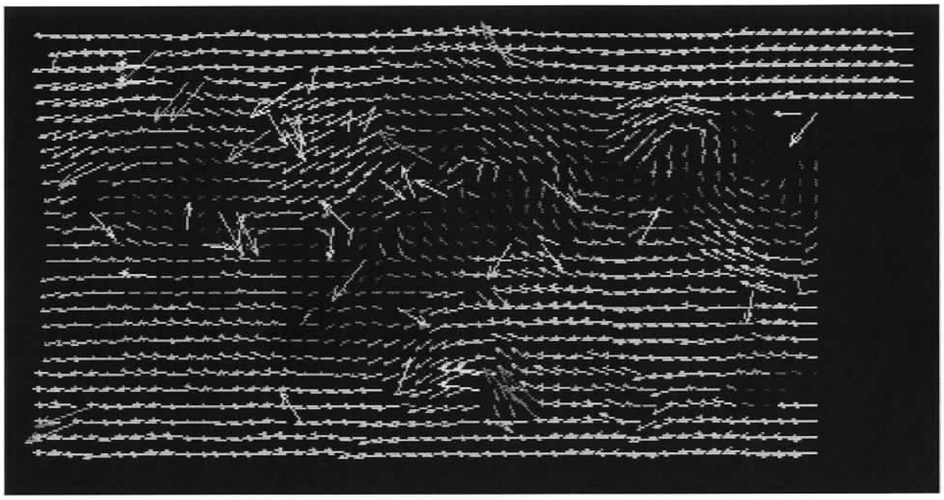

Figure 2.2-5 Typical raw vector field.

2.3 Modeling the phases of the cardiac cycle

As mentioned previously, when considering a single heart valve, the cardiac cycle can be fully represented by four phases: the opening phase, the fully open phase, the closing phase, and the fully closed phase. Each phase exhibits unique fluid phenomena. Out of the four phases of the cardiac cycle, only the fully open and the fully closed valve flow phases will be considered here.

2.3.1 Fully open phase

At the beginning of systole, the left ventricle contracts and forces blood into the aorta, opening the aortic valve. Approximately 10ms after the beginning of systole, the valve is fully open and the average flow velocity has reached 1.35m/s, Yoganathan *et al.* [2], which corresponds to a flow rate of 450ml/s and a Reynolds number of 9500. Although it would be intuitive to use blood as the working fluid, it is hard to preserve and extremely impractical to work with. Hence, water is used as the working fluid for the present study. Maintaining Reynolds number similarity, therefore, requires an average velocity through the valve of 0.34m/s. A 1/6hp pump provided the constant pressure head necessary to maintain a net positive average flow rate of 1.35m/s.

The coordinate system shown in Figure 2.3-1 is used in the analysis presented in later sections. The valve's horizontal axis of symmetry is defined as z = 0 and the valve's vertical axis of symmetry is defined as y = 0. The x = 0 coordinate corresponds to the downstream edge of the valve housing. Flow measurements are not performed within the first 10 millimeters downstream of the valve housing due to optical inaccessibility.

To characterize the three-dimensionality of the flow several parallel planes are used as the data acquisition planes. The first set, positioned along the vertical axis, consisted of five parallel horizontal planes positioned at z = 0, z = 2.6, z = -2.6, z = 8, and z = -8 mm (DAP OL-A through OL-E), as shown in Figure 2.3-1. The second set, positioned along the horizontal axis, consisted of three parallel vertical planes located at x = -10, x = -16, and x = -20 mm (DAP OC-A through OC-C), as shown in Figure 2.3-2.

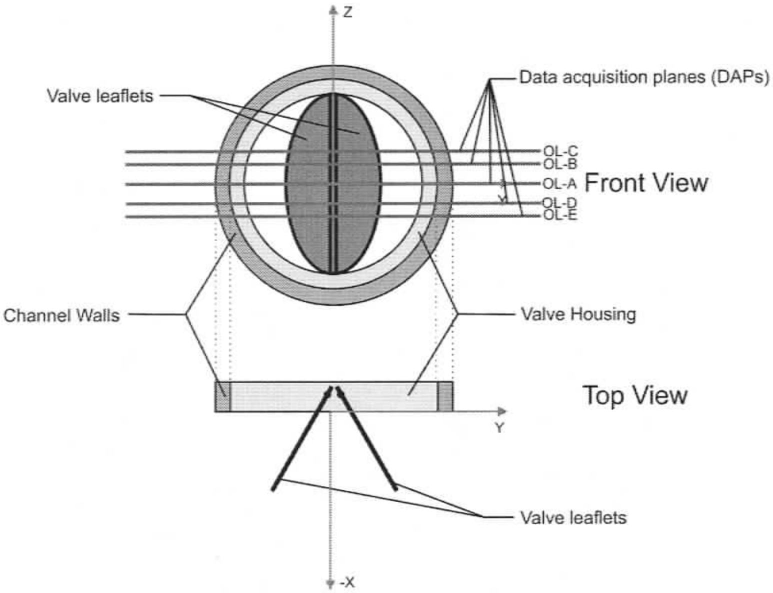

Figure 2.3-1. Definition of coordinate system and longitudinal DAPs for the fully open phase.

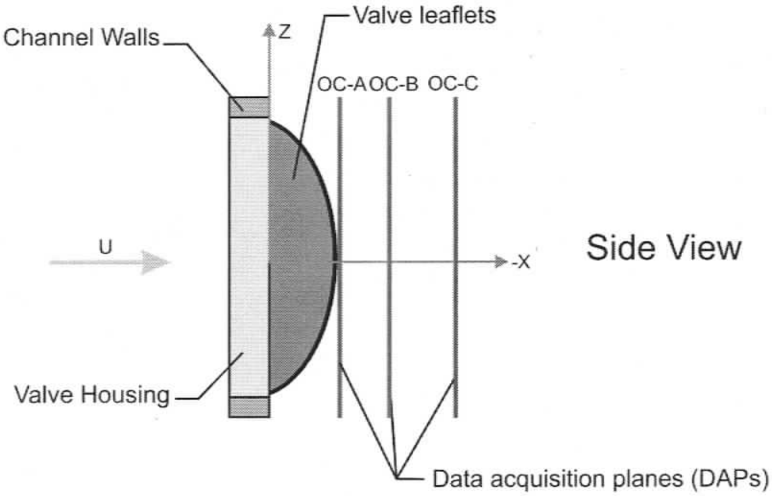

Figure 2.3-2. Definition of coordinate system and cross-sectional DAPs for the fully open phase.

2.3.2 Back flow phase

Throughout the diastole, the aortic valve remains closed and it can be subject to pressures as high as 100mmHg, Yoganathan *et al.* [2]. Previous work by Vivitro Systems (Vivitro, Victoria BC, Canada) provided the amount of regurgitation, or leakage, through several types of mechanical heart valves when subject to physiological loads. According to these measurements, a Carbomedics bileaflet MHV leaks at a rate of 7ml/s when subject to a pressure of 100mmHg. Therefore, a centrifugal 2HP pump is used to provide sufficient pressure to simulate the regurgitant flow.

Two sets of parallel planes are used as the data acquisition planes. The first set, positioned along the vertical axis, consisted of one parallel horizontal plane positioned at the origin of the z-axis (DAP CL-A), as shown in Figure 2.3-3. The second set, positioned along the horizontal axis, consisted of three parallel vertical planes located at x = 4, x = 7, x = 14, and x = 21mm (DAP CC-A through CC-D), as shown in Figure 2.3-4.

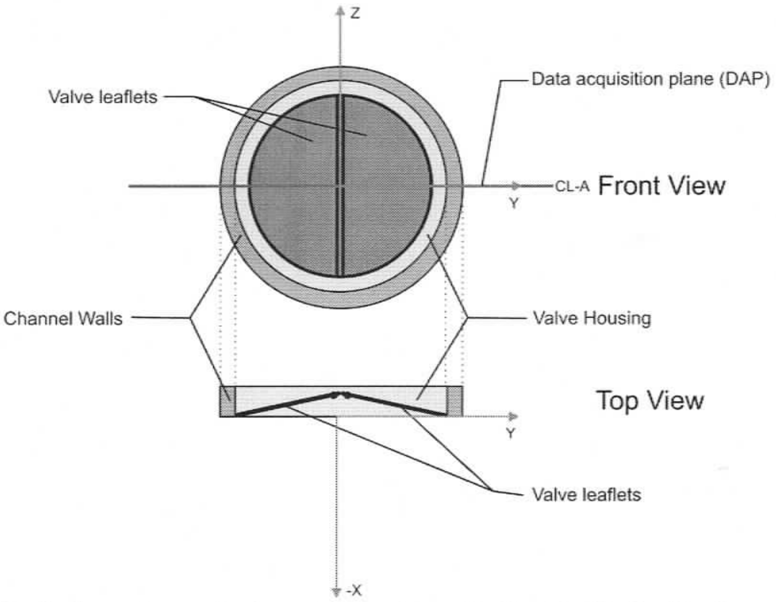

Figure 2.3-3. Definition of coordinate system and longitudinal DAPs for the fully closed phase.

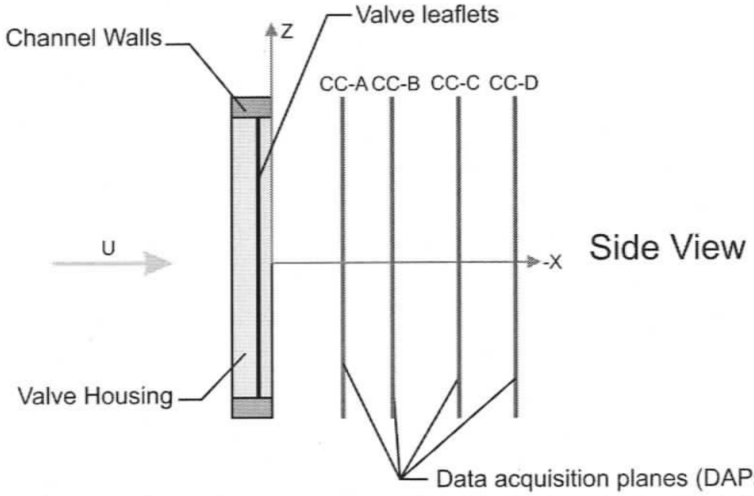

Figure 2.3-4. Definition of coordinate system and longitudinal DAPs for the fully closed phase.

Chapter 3 Forward Flow Phase

A steady-state state investigation of a bileaflet mechanical heart valve (MHV) in the fully open position was conducted using DPIV. The valve was mounted in a Plexiglas cylindrical channel; connected, with flexible tubing, to a 1/6 hp pump. All images were taken at a Reynolds number of 9500, which corresponds to the peak systolic flow rate. In order to characterize the three-dimensionality of the flow several parallel planes are used as the data acquisition planes (DAPs). The first set of DAPs, aligned parallel to the vertical axis of the valve and referred to herein as the longitudinal DAPs, consisted of five parallel horizontal planes positioned at $z = 0$, $z = 2.6$, $z = -2.6$, $z = 8$, and $z = -8$ mm (DAP OL-A through OL-E), as shown in Figure 2.3-1. The second set, positioned along the horizontal axis and referred herein as the cross-sectional DAPs, consisted of three parallel vertical planes located at $x = 10$, $x = 16$, and $x = 21$ mm (DAP OC-A through OC-C), as show in Figure 2.3-2.

3.1 Longitudinal data acquisition planes

All results presented here correspond to a steady unidirectional turbulent inflow from right to left. The red shaded areas outlined in white indicate the leaflets of the fully open valve. The regions between the leaflets as well as those directly above the upper leaflet do not show velocity vectors due to optical inaccessibility.

3.1.1 Instantaneous flow patterns

Plots of instantaneous velocity, $\underline{v}$, and the associated out-of-plane vorticity, ω_z, corresponding to DAPs OL-A, OL-B, and OL-C are shown in Figure 3.1-1 through Figure 3.1-3. The flow patterns corresponding to the DAPs located below the central plane (DAPs OL-D and OL-E) are qualitatively similar to those corresponding to the

DAPs located above the central plane (DAPs OL-B and OL-C). Therefore, for brevity the instantaneous results obtained below the central plane are not shown here.

Generally, the following flow structure is observed downstream of the valve in each of the five horizontal data acquisition planes (DAPs OL-A through OL-E). Shear layers are formed at the tips of both leaflets. The outer shear layers, which form at the trailing edges of the leaflets, roll up into vortices that are shed. It is traditionally assumed that the inner shear layers, which form at the leading edges of the leaflets, roll into vortices that stay attached to the leaflet surface. Present observations indicate that for the case of a unidirectional flow through a fully-open valve, vortex shedding occurs from both the inner and outer tips of the leaflets. The four shear layers define two wake regions, one behind each leaflet. A high velocity jet-like flow region exists between the two wakes. This high-velocity flow will be referred to here as the central jet. The central jet is unsteady in nature. It exhibits a large-scale, low frequency oscillation in the transverse direction. This phenomenon occurs simultaneously with the vortex shedding from the tips of the leaflets. Figure 3.1-1 through Figure 3.1-3 illustrate three characteristic phases of this oscillation observed at DAP OL-A. These phases are referred to as upper central jet regime (Figure 3.1-1), middle central jet regime (Figure 3.1-2), and lower central jet regime (Figure 3.1-3).

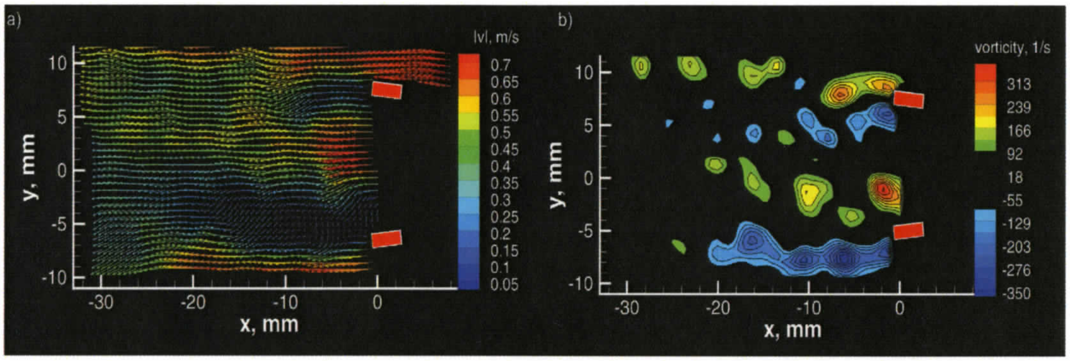

Figure 3.1-1 Instantaneous patterns of velocity (a) and out-of-plane vorticity (b) corresponding to the upward deflection of the central jet during the forward flow phase (DAP OL-A)

Figure 3.1-1 corresponds to the instant in time when the wake from the lower leaflet dominates the flow field and the central jet is deflected upwards. The velocity vector plot shows that the low velocity region corresponding to the lower wake occupies a significantly larger area compared to the upper wake.

In comparison to the upper wake, the lower wake exhibits significantly higher levels of vorticity. The vorticity contour plot, of Figure 3.1-1, shows that the outer shear layer of the bottom leaflet contains three well-defined negative vortices that were shed from the trailing edge of the leaflet. The distance between these negative vortices indicates that their shedding frequency is similar to that of the vortices in the inner shear layer. Moreover, the vortices in the outer and inner shear layers of the lower leaflet retain substantial levels of circulation up to 20 mm downstream of the valve.

In contrast to the lower leaflet, the outer and inner shear layers of the upper leaflet are located significantly closer to each other. In particular, the negative vortices of the inner layer develop close to the leaflet surface and interact with the positive vortices of the outer shear layer by forming counter-rotating vortex pairs. As the counter-rotating vortices move downstream, the interaction between them results in a rapid decrease of their circulation levels. Rapid dissipation of vorticity due to shear layer interaction results in the early collapse of the upper wake, which extends only 10 mm downstream of the valve. This collapse is accompanied by the upward deflection of the inner shear layer of the lower leaflet.

The subsequent characteristic phase of the flow oscillation cycle is referred to as the middle central jet regime and is illustrated by the instantaneous velocity field and out-of-plane vorticity plots shown in Figure 3.1-2. During this phase, the four shear layers do not exhibit significant transverse deflections. Both the upper and lower wakes contain comparable vorticity levels up to 10 mm downstream of the valve. The symmetric wake regime corresponds to the transition between the dominant lower wake phase of Figure 3.1-1 and the dominant upper wake phase, which is illustrated in Figure 3.1-3.

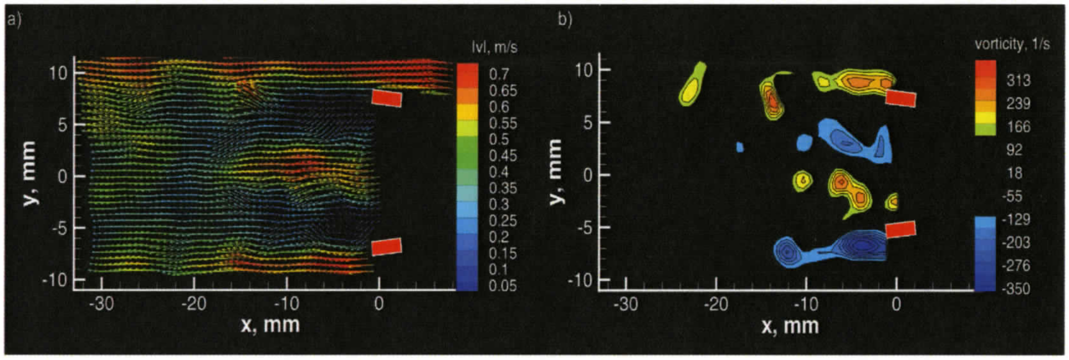

Figure 3.1-2 Instantaneous patterns of velocity (a) and out-of-plane vorticity (b) corresponding to the horizontal position of the central jet during the forward flow phase (DAP OL-A)

Patterns of instantaneous flow velocity and out-of-plane vorticity shown in Figure 3.1-3 correspond to the flow oscillation phase that is opposite to the upper central jet regime of Figure 3.1-1. The velocity field of Figure 3.1-3 shows that the wake region, which forms behind the upper leaflet, dominates the flow field. Rapid dissipation of positive vorticity in the inner shear layer of the lower leaflet is accompanied by a large-scale downward deflection of the inner shear layer of the upper leaflet and the associated jet-like flow in the middle of the channel.

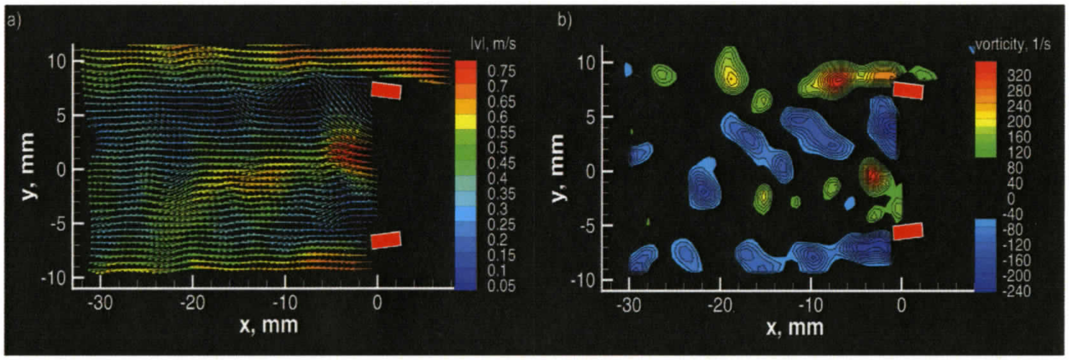

Figure 3.1-3 Instantaneous patterns of velocity (a) and out-of-plane vorticity (b) corresponding to the downward deflection of the central jet during the forward flow phase (DAP OL-A)

It is evident that the frequency of the large-scale flow oscillation represented by the sequence of images in Figure 3.1-1 through Figure 3.1-3 is substantially lower than the frequency of the vortex shedding from the tips of the leaflets. In fact, at least four small-scale vortices are shed from the leaflet tips during a typical large-scale oscillation cycle described above.

Figure 3.1-4 through Figure 3.1-6 show instantaneous velocity fields along with their corresponding out-of-plane vorticity plots at three different time instants taken at DAP OL-B, which is located 2.6 mm above the central plane. The general structure of the flow is similar to that observed at DAP OL-A, with the exception of the fact that the central jet has shifted toward the lower leaflet. Vortices are shed from both the leading edge and the trailing edge of the valve's leaflets. These two pairs of counter rotating vortices define the upper wake and the lower wake. Between the two wakes there is a high-velocity jet-like region, which oscillates in the transverse direction, similar to a planar jet. The central jet's amplitude of oscillation is lower than that observed at DAP OL-A.

The instantaneous velocity field and corresponding out-of-plane vorticity plot of Figure 3.1-4 show upward transverse deflection of the central jet at DAP OL-B. In this plane, the jet remains horizontal during the first 10 mm, before it is deflected. Consequently, the upper wake retains a substantial size over the first 10 mm downstream of the valve. Once the central jet is deflected upwards, the spatial distance between the shed vortices from the leading and trailing tips of the upper leaflet is decreased. The resulting interaction leads to a pronounced reduction in circulation levels of the vortices.

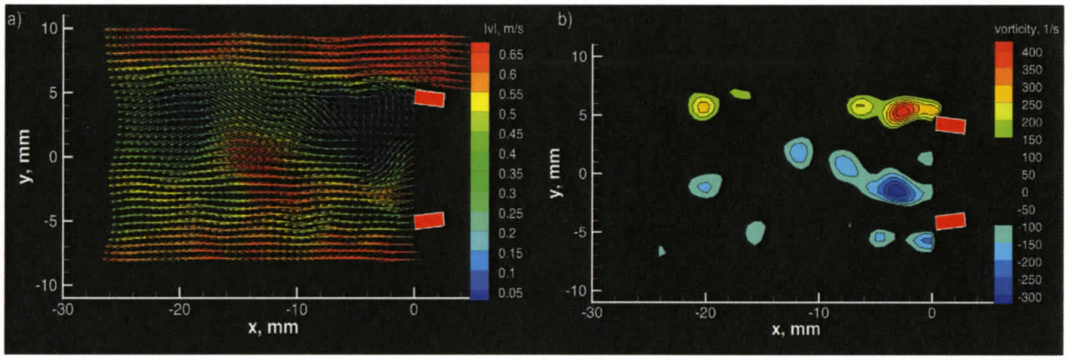

Figure 3.1-4 Instantaneous patterns of velocity (a) and out-of-plane vorticity (b) corresponding to the upward deflection of the central jet during the forward flow phase (DAP OL-B)

The phase corresponding to a horizontal position of the central jet at DAP OL-B is shown in the instantaneous velocity field and the out-of-plane vorticity plot of

Figure 3.1-5. Neither the central jet nor the shear layers show evidence of a large-scale transverse deflection. Both wakes retain significant levels of vorticity up to 14 mm downstream of the valve. In comparison, the area of the upper wake is larger than that of the lower wake. This effect can be accounted solely by the shift of the central jet toward the lower leaflet, which becomes more pronounced with increasing distance along the vertical axis.

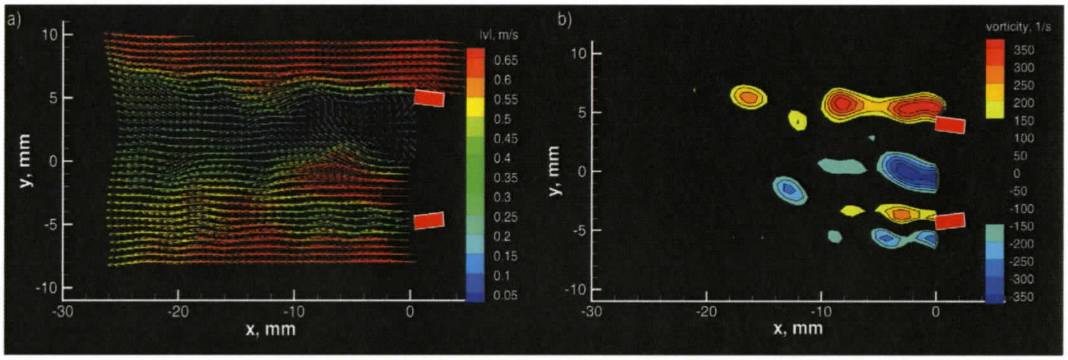

Figure 3.1-5 Instantaneous patterns of velocity (a) and out-of-plane vorticity (b) corresponding to the horizontal position of the central jet during the forward flow phase (DAP OL-B)

Figure 3.1-6 shows the instantaneous velocity field and out-of-plane vorticity plot corresponding to the upward oscillation of the central jet obtained at DAP OL-B. The central jet is deflected downward reducing the distance between the vortices that are shed from the lower leaflet. Since the initial distance between the shed vortices from the leading and trailing edge of the lower leaflet is small, a downward deflection of the central jet results in a very rapid reduction of circulation levels in the lower wake. In fact, levels of vorticity in the lower wake are virtually negligible 10 mm downstream of the valve.

Figure 3.1-7, Figure 3.1-8, and Figure 3.1-9 show instantaneous velocity fields at three different instants in time taken at DAP OL-C. The general structure of the flow is similar to that observed in DAP OL-A and DAP OL-B. However, the central jet is located even closer to the lower leaflet. The overall velocity magnitudes are lower due to the proximity to the channel walls. The upper wake remains the dominant feature of the flow field, and the amplitude of the jet's oscillation is slightly lower than that observed in DAP OL-B.

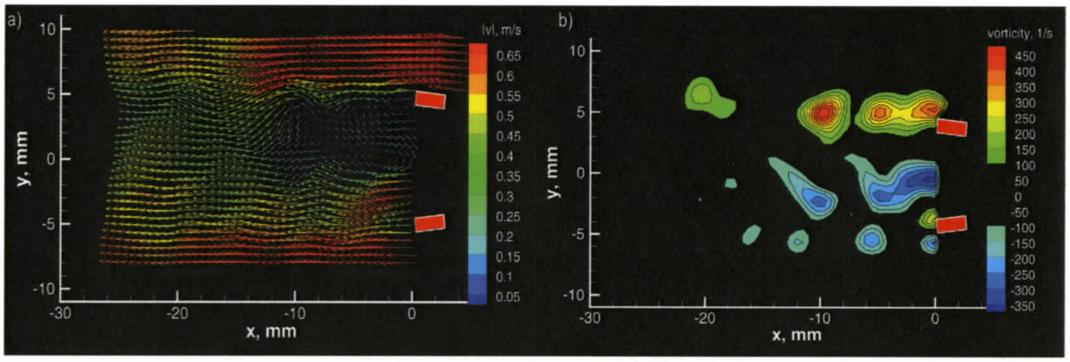

Figure 3.1-6 Instantaneous patterns of velocity (a) and out-of-plane vorticity (b) corresponding to the downward deflection of the central jet during the forward flow phase (DAP OL-B)

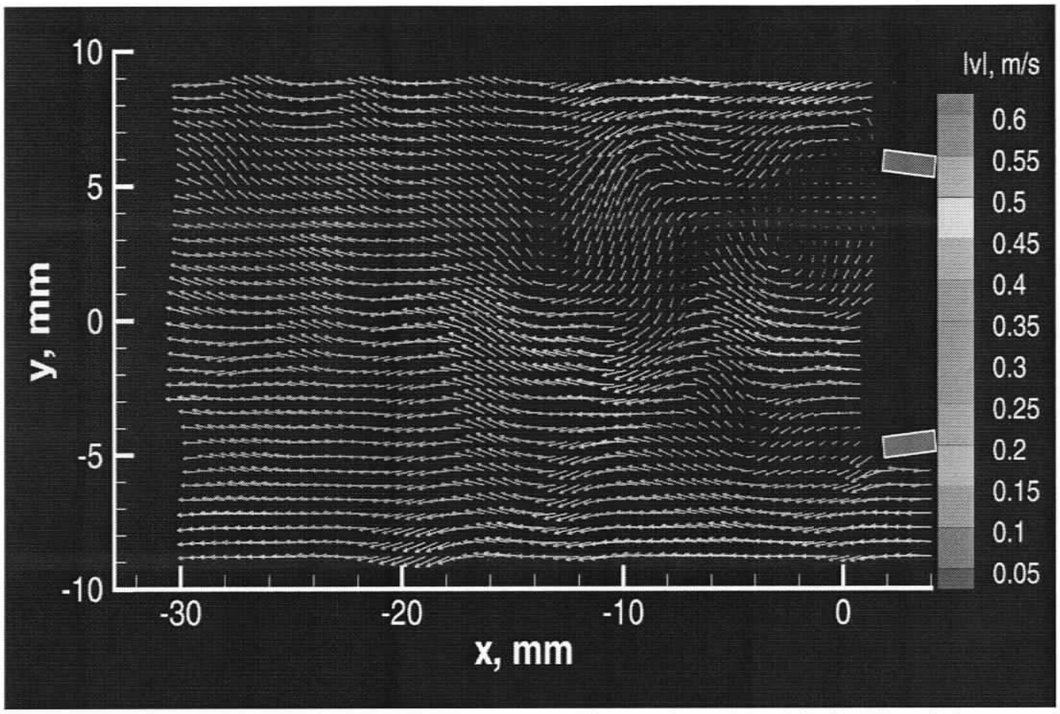

Figure 3.1-7. Instantaneous velocity field corresponding to the upward deflection of the central jet during the forward flow phase (DAP OL-C)

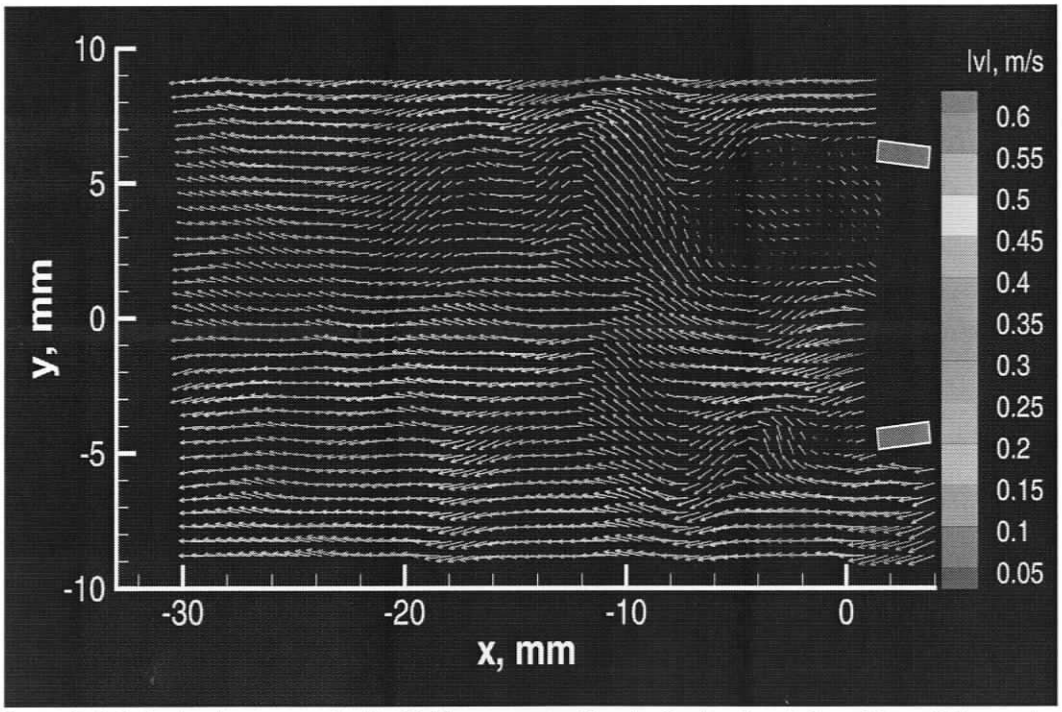

Figure 3.1-8. Instantaneous velocity field corresponding to the horizontal position of the central jet during the forward flow phase (DAP OL-C)

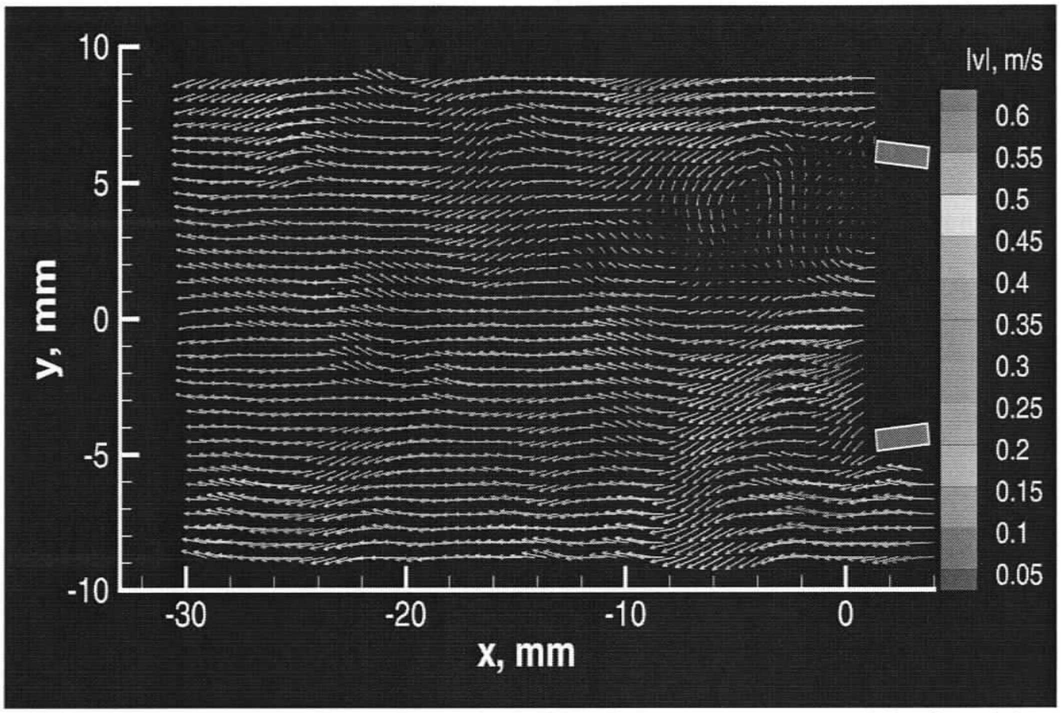

Figure 3.1-9. Instantaneous velocity field corresponding to the downward deflection of the central jet during the forward flow phase (DAP OL-C)

3.1.2 Time-averaged flow patterns

All images presented in this section are a result of ensemble averaging of 1000 instantaneous images similar to those presented in the previous section.

The structure of the wake downstream of the bileaflet MHV, corresponding to DAP OL-A, is clearly evident in the plot of time-averaged vorticity $<\omega_z>$ of Figure 3.1-10. The dominant feature of the flow field downstream of the valve is the presence of four separated shear layers that form at the tips of the leaflets. The outer shear layers form at the trailing tips of the upper and lower leaflet. They are indicated in the plot of out-of-plane vorticity of Figure 3.1-10 by the regions of high positive and negative time-averaged vorticity respectively. These layers extend approximately 14 mm downstream of the valve. The inner shear layers, which form at the leading tips of the leaflets, exhibit high levels of time-averaged vorticity of the opposite sign, relative to the outer shear layers. Due to the highly unsteady nature of the inner shear layers, the time-averaged vorticity associated with them decreases rapidly with downstream distance. In fact, no significant levels of vorticity exist in the central region of the channel downstream of the valve beyond 6mm, approximately.

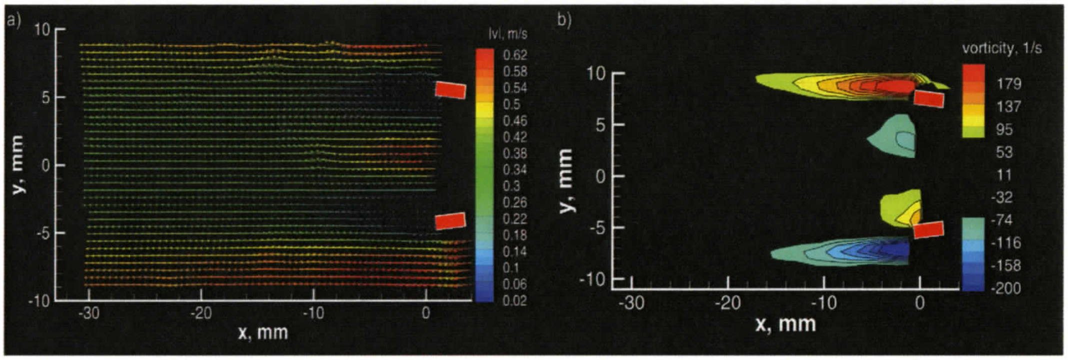

Figure 3.1-10 Time-averaged velocity field (a) and corresponding out-of-plane vorticity (b) during the forward flow phase (DAP OL-A)

The time-averaged velocity field and the corresponding out-of-plane vorticity plot for DAP OL-B are shown in Figure 3.1-11. Once again, the dominant feature of the flow field downstream of the valve is the presence of four separated shear layers that originate at the tips of the leaflets. However, the central jet has shifted toward the lower leaflet causing an asymmetry in the flow structure. The inner and outer shear layers that define the relatively large upper wake are formed at the leading and trailing edges of the top leaflet. They are represented, in Figure 3.1-11, by high levels of out-of-plane vorticity that extend 14 mm downstream of the valve. In contrast, the relatively small lower wake, which is defined by the inner and outer shear layers formed at the leading and trailing edges of the lower leaflet, contains lower circulation levels that only extend 10mm downstream of the valve. The shift in the central jet's position reduces the distance between the shear layers that define the lower wake, causing them to interact. This interaction results in reduced levels of circulation in the lower wake as well as higher Reynolds stresses.

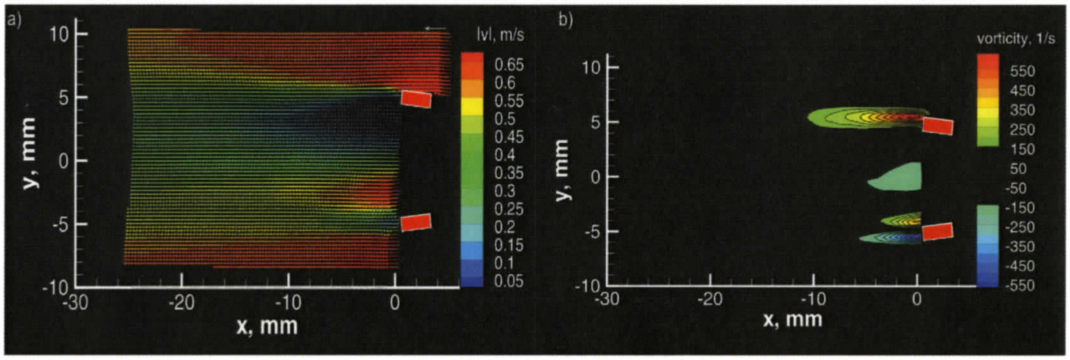

Figure 3.1-11 Time-averaged velocity (a) and corresponding out-of-plane vorticity (b) during the forward flow phase (DAP OL-B)

DAP OL-C, which corresponds to a further increase in the distance from the centerline of the channel, shows a very similar flow structure as that of DAP OL-B. As can be seen in Figure 3.1-12, the upper wake dominates the lower wake and the central jet has shifted toward the lower leaflet. In comparison to the results of DAP OL-B, the overall velocity magnitude is lower for DAP OL-C due to the proximity to the channel walls. Consequently, the size of both the upper wake and the lower wake decreases by the same amount. Figure 3.1-13 shows a plot of wake size as a function of radial distance from the channel centerline.

The flow directly downstream of the bileaflet MHV is highly three-dimensional. Marked differences are found in the flow structure downstream of the MHV at each DAP. Predominantly, the central jet shifts position along the vertical axis, causing an increase in the size of one wake and a reduction in size of the other.

In general, the shift of the central jet causes a significant change in the unsteady flow structures present downstream of the valve.

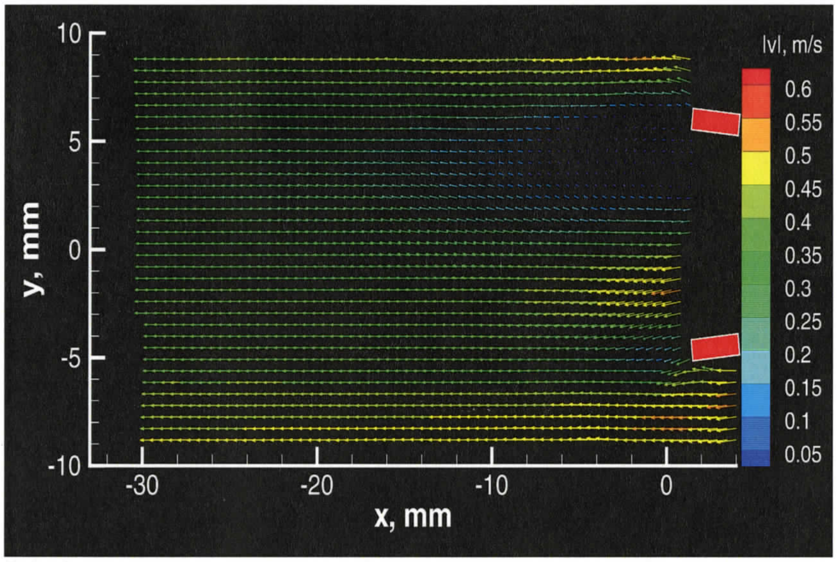

Figure 3.1-12. Time-averaged velocity field during the forward flow phase (DAP OL-C)

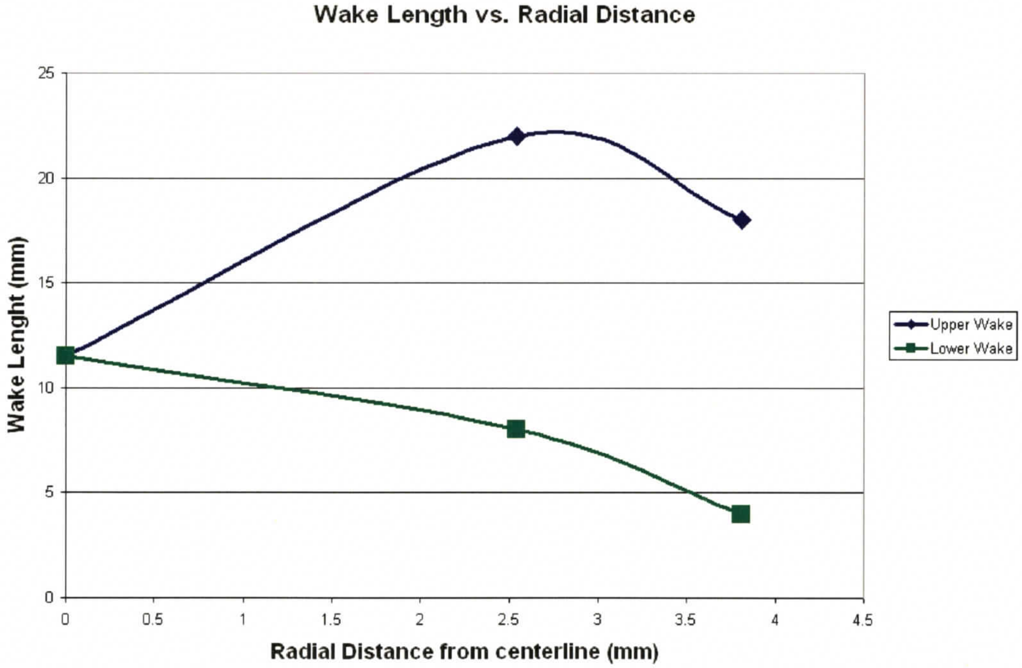

Figure 3.1-13 Wake size as a function of distance along the y-axis corresponding to a symmetric wake regime downstream of the valve at DAP OL-A.

The observed asymmetry, however, is not only a function of displacement along the vertical axis. Further data acquisition at DAP OL-A showed a pronounced asymmetry similar to that previously presented as happening at DAP OL-B and OL-C. This result, combined with a non-bias experimental set-up, suggests the position of the valve's leaflets is not entirely repeatable. In other words, current evidence points to an asymmetrical opening of the valve's leaflets.

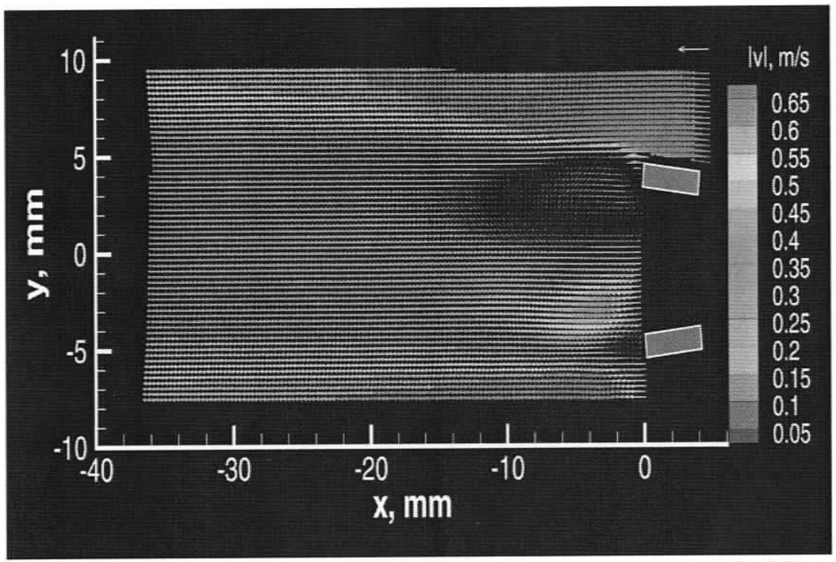

Figure 3.1-14. Time-averaged velocity field corresponding to an asymmetrical flow structure downstream of the open valve during the forward flow phase (DAP OL-A)

Figure 3.1-14 shows time-averaged velocity field corresponding to an asymmetric time-averaged flow regime in DAP OL-A. The overall flow structure remains similar to that shown in Figure 3.1-10. Four separated shear layers dominate the flow field, which define the upper and lower wake. Between the two wakes, a high-speed jet-like region is observed.

The central jet's position, however, is no longer in the middle of the two leaflets but has shifted toward the lower leaflet. As before, the shift of the central jet's position reduces the distance between the shear layers that define the lower wake, causing them to interact. On the other hand the distance between the shear layers that define the upper wake is increased and results in the upper wake dominating the flow field. The upper wake extends up to 14mm downstream of the valve while the lower wake only extends up to 5mm downstream of the valve.

Further results for DAP OL-B through OL-E showed the flow structure is similar at every DAP. However, there is a marked variation in the sizes of both the upper and lower wake at each DAP. Figure 3.1-15 shows a plot of wake size as a function of vertical distance.

A comparison of the results presented in Figure 3.1-13 and Figure 3.1-15 shows a marked difference in the three-dimensional structure of the central jet and the upper and lower wakes. In Figure 3.1-13, both the upper and lower wake are the same size at DAP OL-A with the central jet lying exactly in the middle of the two wakes. The upper wake grows in size and the lower wake decreases in size as distance along the y-axis increases. At DAP OL-B both the upper and lower wakes reduce in size due to proximity to the channel walls. However, the upper wake remains dominant.

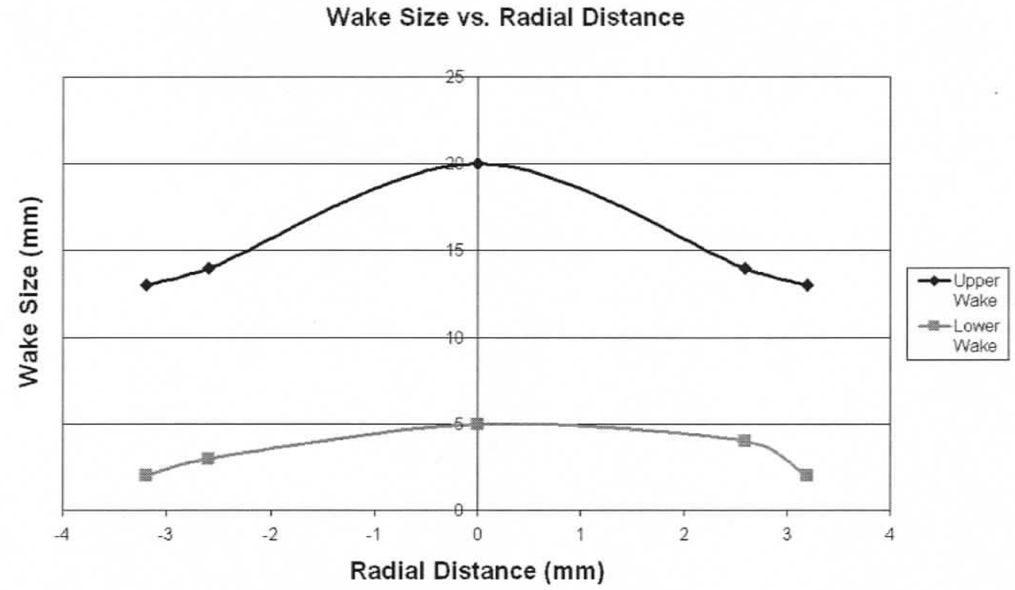

Figure 3.1-15. Wake size as a function of distance along the y-axis corresponding to an asymmetric wake regime downstream of the valve at DAP OL-A

On the other hand, the upper wake remains dominant along the entire y-axis as shown in Figure 3.1-15. Both the upper and lower wakes reach their maximum size at the centerline and reduce in size closer to the channel walls.

Figure 3.1-16 show patterns of velocity fluctuations in the wake of the valve in terms of root-mean-square of horizontal and vertical velocity components, respectively. High levels of u_{rms} are associated with the unsteadiness of the inner shear layers and the periodic growth and collapse of the wakes of the leaflets. The peak levels of u_{rms} of 0.2 m/s occur at the locations of the separation of the inner shear layers. Significant levels of u_{rms} are observed as far as 22 mm downstream of the valve. Peak values of v_{rms} of 0.12 m/s also occur at the location of the separation of the inner shear layers. Elevated values of v_{rms} are also associated with transverse undulations of the outer shear layers.

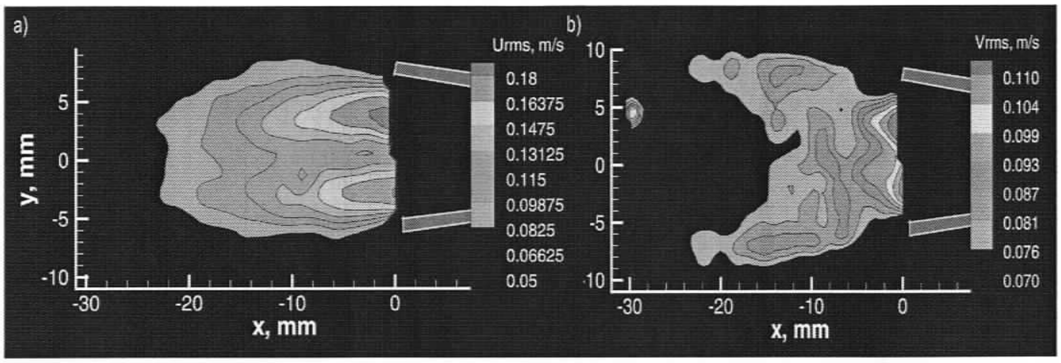

Figure 3.1-16 Root-mean-square of streamwise (a) and radial (b) velocity component corresponding to a symmetric flow structure downstream of the fully open valve (DAP OL-A)

The distribution of the velocity correlation <u′v′>, which corresponds to the dominant Reynolds shear stress component, obtained at DAP OL-A and corresponding to a symmetrical flow structure downstream of the open valve, is shown in Figure 3.1-17. Elevated values of <u′v′> are associated with the inner shear layers and the downstream sections of the outer shear layers. The peak values of ±0.01 m^2/s^2 occur in the near-wakes of the leaflets. Although limited temporal resolution of the DPIV imaging sequence did not allow for the calculation of pathlines and hence the accurate evaluation of the platelet activation state (PAS), the plot of Figure 3.1-17 provides an indication of the regions within the wake of the bileaflet valve that contribute the most to the platelet activation.

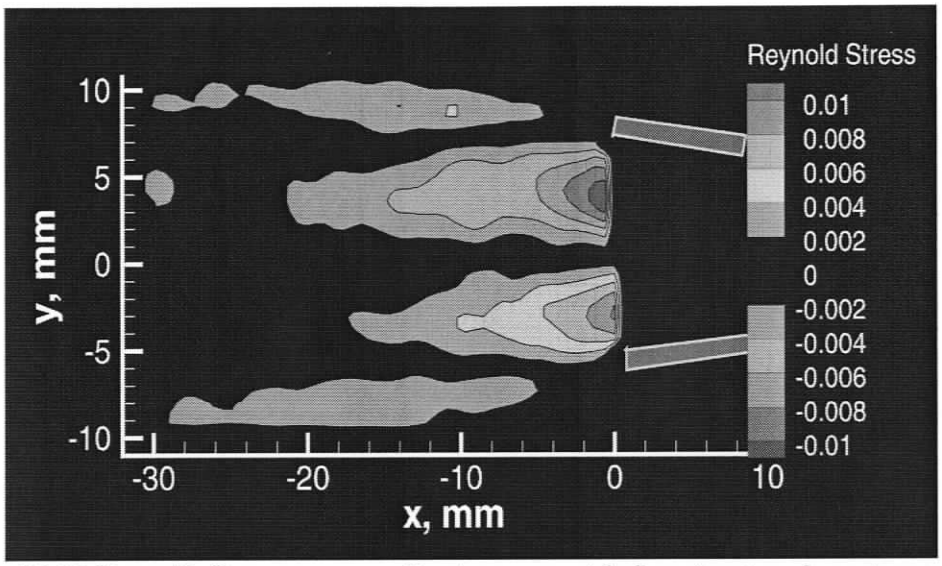

Figure 3.1-17. Reynolds Stress corresponding to a symmetric flow structure downstream of the fully open valve (DAP OL-A)

Figure 3.1-18 shows the Reynolds shear stress correlation, obtained at DAP OL-A and corresponding to an asymmetrical flow structure downstream of the MHV. The highest levels <u′v′> are associated with the shear layers of the top leaflet, while the shear layers of the bottom leaflet exhibit relatively low Reynolds shear stress levels. In comparison to the results obtained when the flow structure downstream of the open valve is symmetrical, the peak levels of <u′v′> are approximately 30% lower.

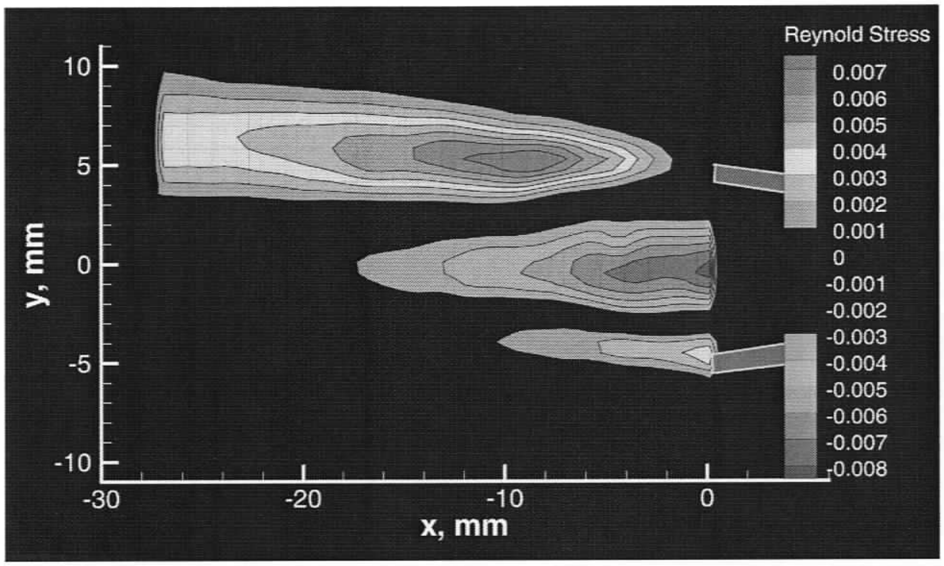

Figure 3.1-18 Reynolds Stress corresponding to an asymmetric flow structure downstream of the fully open valve (DAP OL-A)

Figure 3.1-19 shows the Reynolds shear stress correlation obtained at DAP OL-B, located 2.6mm along the z-axis. Peak levels are only slightly lower than those of DAP OL-A. Levels of <u'v'> associated with the shear layers of the lower leaflet are virtually negligible, while the levels associated with the shear layers of the top leaflet dominate the flow field.

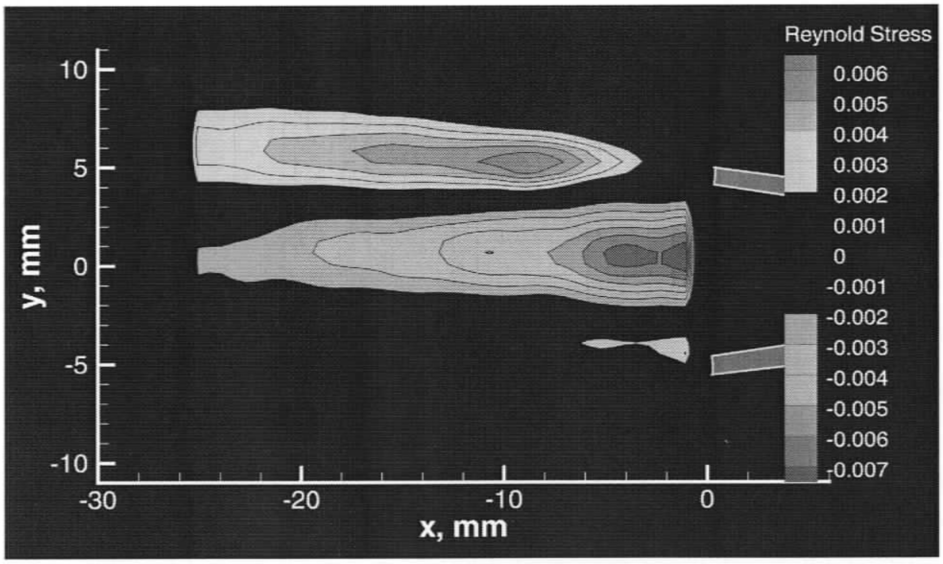

Figure 3.1-19 Reynolds Stress downstream of the fully open valve (DAP OL-B)

3.2 Cross-stream data acquisition planes

The images in this section correspond to cross-stream cuts of the flow field. The bulk flow is directed out of the image plane. The valve's leaflets are not shown. Moreover, images could not be obtained in the first 10 mm downstream of the valve's housing due to optical inaccessibility.

3.2.1 Instantaneous flow patterns

Figure 3.2-1 shows the instantaneous velocity field and the corresponding out-of-plane vorticity plot for DAP OC-A, obtained 1 mm downstream of the tip of the valve's leaflets. The two side openings, located between the leaflets and the channel walls, are the sources of two high-speed jet-like regions, referred to here as the side jets. The presence of the central opening, located between the two leaflets of the open valve, results in formation of a high-velocity region, referred to here as the central jet. The region between the two leaflets of the open valve exhibits high radial velocities, while the region close to the periphery of the channel exhibit relatively low radial velocities. The high-velocity regions in the cross-stream data acquisition planes (DAP OC-A through DAP OC-C) represent transverse deflections of the downstream moving fluid. The transverse oscillations in x-y and z-y planes are discussed in section 3.1.

A total of five distinguishing flow features are identified in the velocity field of Figure 3.2-1. The first distinguishing feature corresponds to four high radial velocity regions that are located close to the top and the bottom of the channel. These regions correspond to the outlined areas labeled A, B, C, and D in the schematic of Figure 3.2-2.

Regions A, B, C, and D correspond to the deflection of the side jets by the leaflets. The leaflets have a semicircular shape. Consequently, the path of least resistance for the fluid moving through the side openings (i.e. the side jets) corresponds to the path where the leaflets protrude the least into the flow. Therefore, the side jets are deflected away from the $z = 0$ line and towards the periphery of the channel.

On the other hand, the central jet is defined on both sides by wakes that are created by the presence of the leaflets. In turn, each wake is defined by a pair of counter-rotating vortices that are shed from the tips of each leaflet (refer to section 3.1 for a detailed description of the longitudinal flow structure of the fully open valve). The central jet and the shed vortices are unsteady in nature. They are located in region E (Figure 3.2-2). Pronounced deflections of the central jet and the wakes take place within this region. Overall, the flow structure within region E is unsteady, highly turbulent, and fully three-dimensional. Therefore, a time-resolved investigation of the cross-sectional planes, for the case of the fully open valve would be necessary to completely characterize this flow.

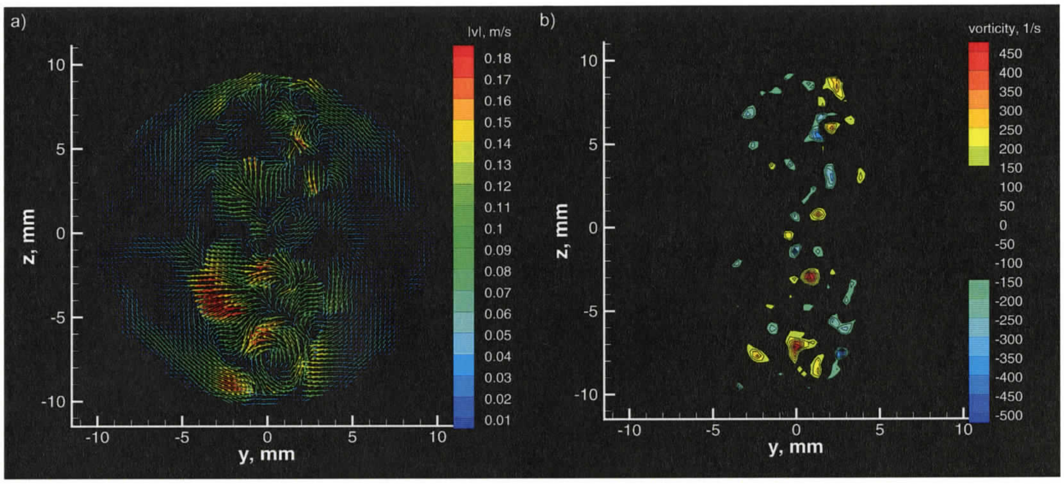

Figure 3.2-1 Instantaneous velocity field (a) and corresponding out-of-plane vorticity plot (b) for the case of fully open valve (DAP OC-A)

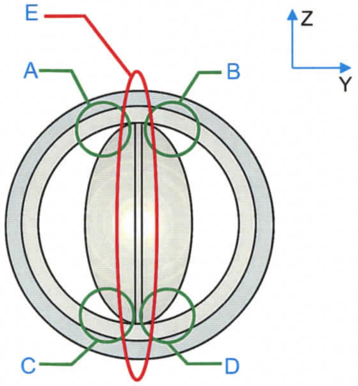

Figure 3.2-2 Schematic of distinguishing flow features downstream of the fully open valve at DAPs OC-A through DAP OC-C

The plot of out-of-plane vorticity of Figure 3.2-1 shows the highest circulation levels are associated with the unsteadiness of the central jet. Peak circulation levels are of the same order of magnitude as those found for the longitudinal planes of the fully open valve (DAP OL-A through DAP OL-E that are discussed in details in Section 3.1).

Figure 3.2-3 shows an instantaneous velocity field and the corresponding out-of-plane vorticity plot for DAP OC-B, obtained 16 mm downstream of the valve. Regions of high velocity correspond to the deflection of the side jets toward the center of the channel. A large number of small-scale vortices, corresponding to the fully turbulent structure of region E, are represented in the vorticity plot of Figure 3.2-3. The typical levels of vorticity exhibited by these structures are approximately 300 s^{-1}.

Figure 3.2-4 shows an instantaneous velocity field and the corresponding out-of-plane vorticity pattern obtained 21 mm downstream of the valve's housing (DAP OC-C.) Peak radial velocity magnitudes remain at the same level as in the previous two planes. The fully-turbulent flow structure originally confined to region E has dissipated into the regions of low radial velocities. Combined with a reduction on peak recirculation levels, a reduction in the levels of radial velocity magnitudes indicates the development of a fully-turbulent pipe flow.

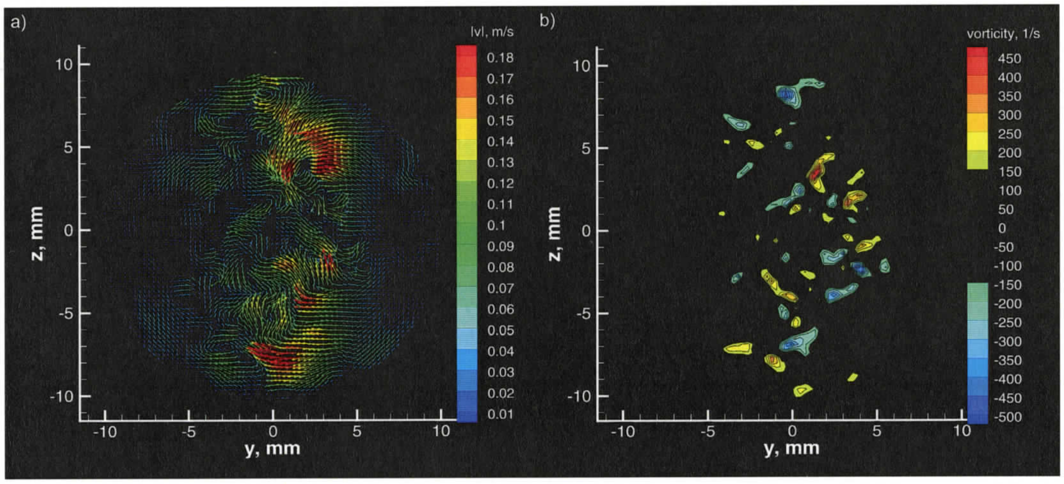

Figure 3.2-3 Instantaneous velocity field (a) and corresponding out-of-plane vorticity plot (b) for the case of fully open valve (DAP OC-B)

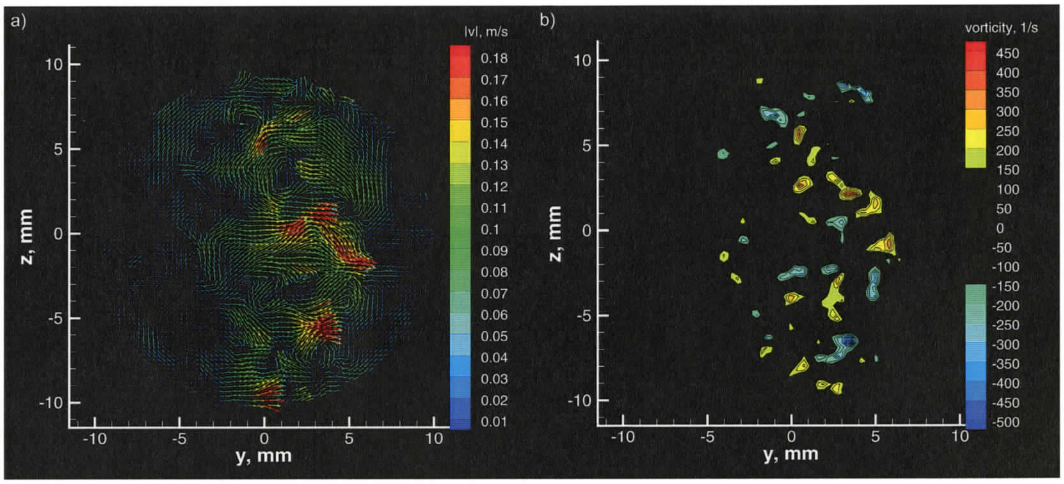

Figure 3.2-4 Instantaneous velocity field (a) and corresponding out-of-plane vorticity plot (b) for the case of fully open valve (DAP OC-C)

3.2.2 Time-averaged flow patterns

All images presented in this section are obtained by ensemble averaging of 1000 instantaneous images that are similar to those presented in the previous section.

Figure 3.2-6 shows the time-averaged velocity field and the corresponding out-of-plane vorticity plot obtained at DAP OC-A, 1 mm downstream of the leaflets' tips. The structure of the flow downstream of the open valve is clearly evident in the velocity field of Figure 3.2-6. Three dominant flow features are observed. The first feature corresponds to the fluid that moves around the leaflets of the open valve, (regions A, B, C, and D of Figure 3.2-2). This structure represents the deflection of the side jets away from the valve's horizontal axis of symmetry.

The second distinguishing flow feature corresponds to the transverse deflection of the central jet in the x-y plane. It is represented in the velocity field of Figure 3.2-6 by the vectors located in region F (Figure 3.2-5.). This flow feature, in the time-averaged sense, corresponds to the flow asymmetry observed as DAP OL-A through DAP OL-E (refer to section 3.1 for a detailed discussion of the results obtained at DAP OL-A through DAP OL-E). In Figure 3.2-6, the deflection of the central jet is represented by a uniform layer of fluid with a characteristic velocity of 0.7 m/s along the left leaflet.

The distinguishing feature, shown in the region of the velocity field of Figure 3.2-6 by the vectors located in region G (Figure 3.2-5), represents the flow redirected from regions A through D. The fluid that passed through the latter regions impinged on the channel walls and is reflected towards the middle of the channel. Only two flow structures are observed within the region G, as the streams that originated from region A and C have merged with the streams from region B and D, respectively.

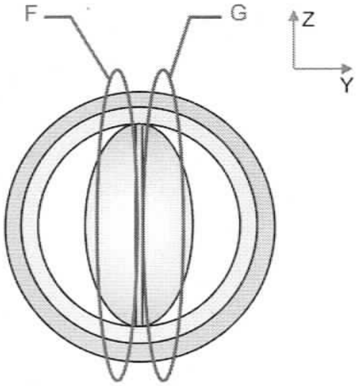

Figure 3.2-5 Schematic of distinguishing flow features downstream of the fully open valve at DAPs OC-A through DAP OC-C

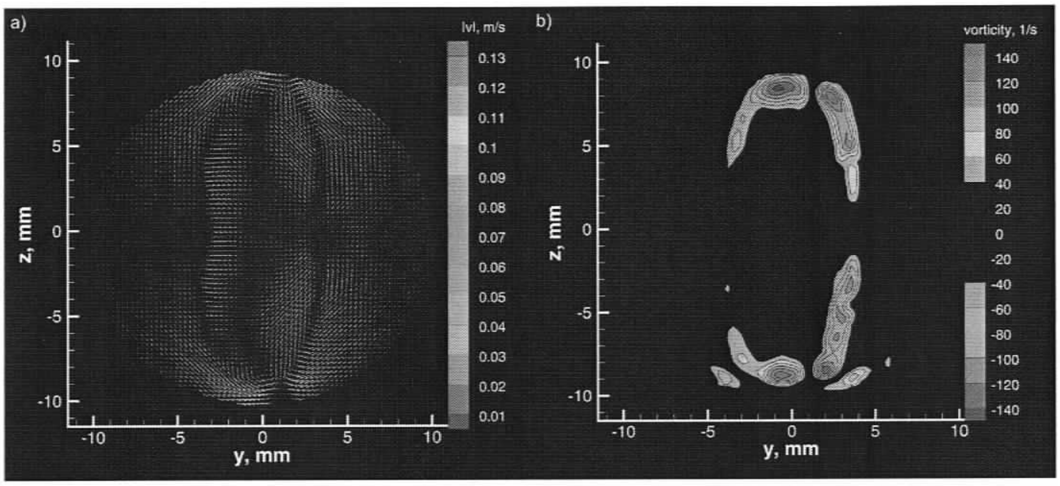

Figure 3.2-6 Time-averaged velocity field (a) and corresponding out-of-plane vorticity plot (b) for the case of fully open valve (DAP OC-A)

Figure 3.2-7 shows the time-averaged velocity field and the corresponding out-of-plane vorticity plot for DAP OC-B, obtained 6 mm downstream of the leaflets' tips. The structure of the flow remains similar to that observed at DAP OC-A, with the exception of the fact that the transverse deflection of the central jet is no longer evident.

The flow features that correspond to regions F and E of Figure 3.2-5 and regions A, B, C, and D of Figure 3.2-2, are still present. In comparison to DAP OC-A, the peak velocities measured at DAP OC-B are approximately 40% lower. Similarly, the vorticity levels at DAP OC-B are approximately 45% lower in comparison to those observed at DAP OC-A. Reduction in magnitude of the radial velocity components is associated with the development of a fully turbulent pipe flow downstream of the open MHV.

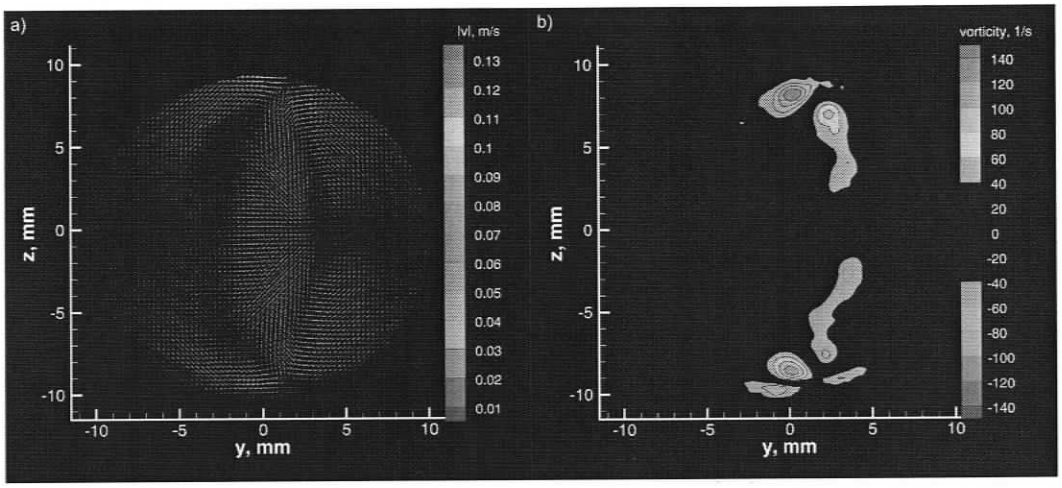

Figure 3.2-7 Time-averaged velocity field (a) and corresponding out-of-plane vorticity plot (b) for the case of fully open valve (DAP OC-B)

A further decrease in the magnitude of radial velocities and vorticity levels is observed at DAP OC-C. Figure 3.2-8 shows the time-averaged velocity field and corresponding out-of-plane vorticity plot obtained 21 mm downstream of the valve, at DAP OC-C.

The flow structures that were identified at DAP OC-B are still present at DAP OC-C. However, both velocity and vorticity magnitudes have decreased to negligible levels. At this location, 21 mm downstream of the valve, the fluid travels primarily along the x-axis.

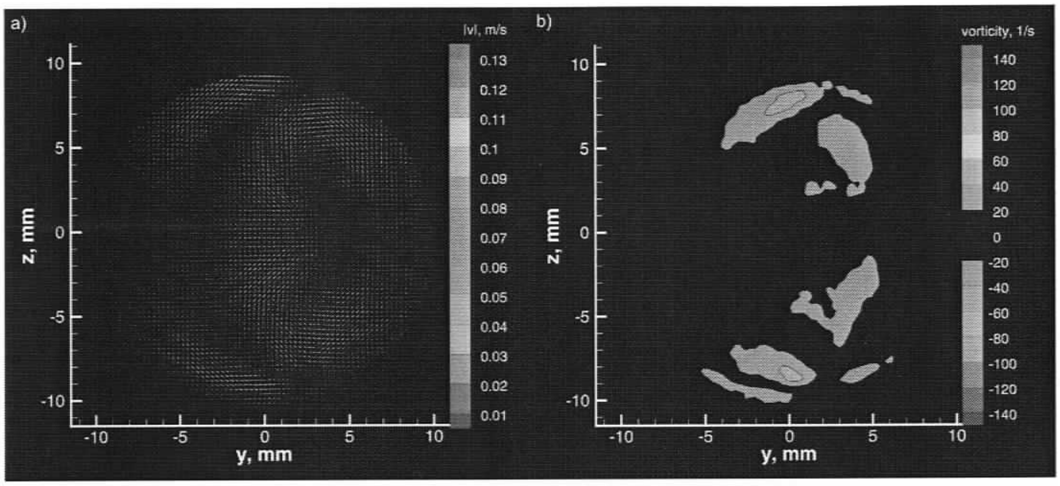

Figure 3.2-8 Time-averaged velocity field (a) and corresponding out-of-plane vorticity plot (b) for the case of fully open valve (DAP OC-C)

The distribution of the velocity correlation <u′v′>, which corresponds to the dominant Reynolds shear stress component, obtained at DAP OC-A is shown in Figure 3.2-9. Peak levels of <u′v′> correspond to the deflection of the side jet away from the center of the channel. The associated regions of Figure 3.2-9 correspond to the areas A, B, C, and D (Figure 3.2-2).

Figure 3.2-10 and Figure 3.2-11 show the dominant Reynolds shear stress components obtained at DAP OC-B and DAP OC-C, respectively. Peak <u′v′> levels are associated with the regions along the channel's vertical axis of symmetry.

Although limited temporal resolution did not allow the calculation of pathlines, the results presented here provide an insight into the structure the flow features that could potentially contribute to platelet activation.

Patterns of velocity fluctuations downstream of the valve were analyzed in terms of root-mean-square of velocity components (not shown here). In general, the region between the valve's leaflets corresponds to the highest levels of flow unsteadiness.

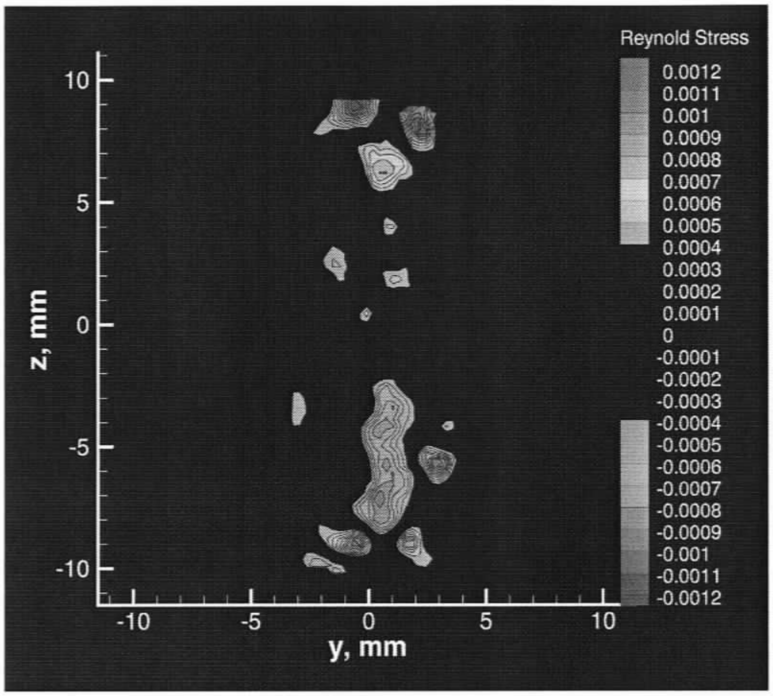

Figure 3.2-9. Reynolds Stress correlation for the case of the fully open valve (DAP OC-A)

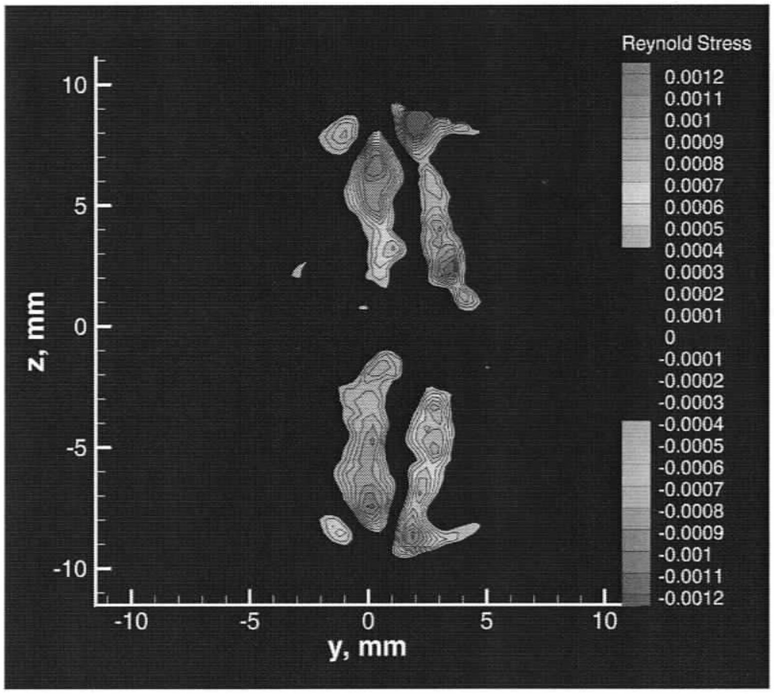

Figure 3.2-10. Reynolds Stress correlation for the case of the fully open valve (DAP OC-B)

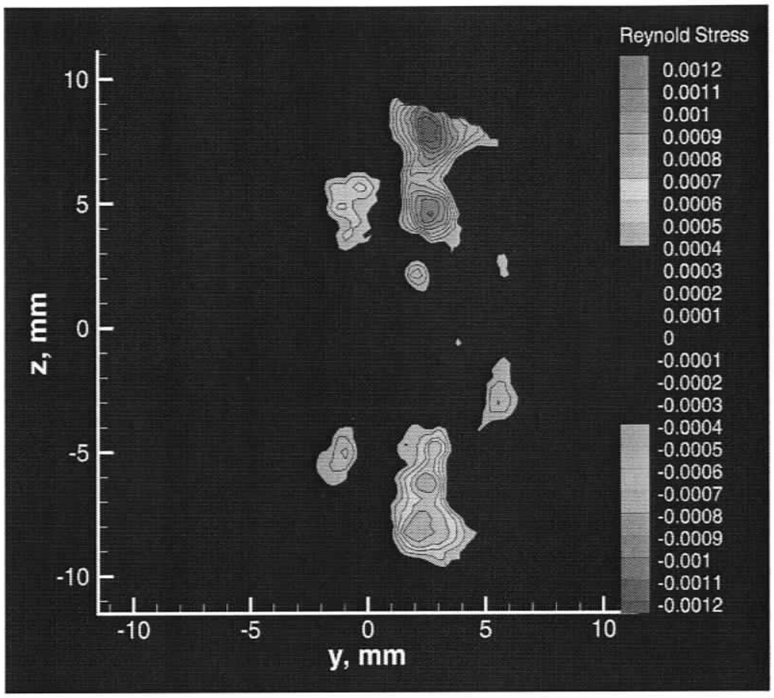

Figure 3.2-11. Reynolds Stress correlation for the case of the fully open valve (DAP OC-C)

Chapter 4 Back Flow Phase

A steady-state state investigation of a bileaflet mechanical heart valve (MHV) in the fully closed position was conducted using DPIV. The valve was mounted in a Plexiglas cylindrical channel; connected to a 2 hp centrifugal pump with flexible tubing. The pressure drop across the valve is adjusted to produce the regurgitant flow rate of 7 ml/sec. The measurements were conducted over several parallel data acquisition planes (DAPs). The first set of DAPs, positioned along the vertical axis of the valve, consisted of one horizontal plane positioned at the origin of the z-axis (DAP CL-A), as shown in Figure 2.3-3. The second set, positioned along the horizontal axis, consisted of four parallel vertical planes located at $x = 4$, $x = 7$, $x = 14$, and $x = 21$ mm (DAPs CC-A through CC-D), as show in Figure 2.3-4.

4.1 Longitudinal Planes of View

The results presented in this section correspond to a steady unidirectional turbulent inflow from right to left. The red shaded areas outlined in white indicate the leaflets of the fully closed valve.

4.1.1 Instantaneous flow patterns

Patterns of instantaneous velocity $\underline{v}$, and the associated out-of-plane vorticity ω_z, corresponding to DAP CL-A are shown in Figure 4.1-1 through Figure 4.1-3. A fully turbulent flow with several recirculation regions is observed downstream of the closed valve. Vortices are shed from both the inner and outer edges of each leaflet. A high-speed jet-like flow, referred to here as the central jet, emerges between the two closed leaflets.

The central jet is unsteady in nature. It exhibits a large-scale, low frequency oscillation in the transverse direction. This phenomenon occurs simultaneously with the vortex shedding from the edges of the leaflets. Figure 4.1-1 through Figure 4.1-3 illustrate three characteristic phases of this oscillation that correspond to DAP CL-A. These phases are referred to as upward deflection of the central jet (Figure 4.1-1), horizontal position of the central jet (Figure 4.1-2), and downward deflection of the central jet (Figure 4.1-3).

In addition to the leakage observed at DAP CL-A, a substantial amount of fluid leaks through the hinges of the valve (refer to section 4.2 for a discussion on the leakage from the hinges of the bileaflet MHV). The regurgitant flow from the hinges of the valve develops into an axial spiral flow, approximately 21 mm downstream of the valve. As the fluid leaks through the valve, a net mass flow is produced in the downstream direction. However, conservation of mass requires the advection of a low-speed bulk flow in the upstream direction. The shed vortices and the central jet, whose general motion is in the downstream direction, collide with the bulk of upstream-moving flow causing an abrupt shift in the trajectory of the upstream-moving fluid.

The instantaneous velocity field of Figure 4.1-1 corresponds to the instant in time when the central jet shows an upward transverse deflection. Vortices shed from the inner edges of the leaflets advect on both sides of the central jet and are also deflected upwards. The upstream bulk flow collides with the downstream moving jet and its accompanying vortices, which results in a downward deflection of the bulk flow. This collision results in low velocity regions located at the interface between the upstream bulk flow and the jet, referred to here as the *bulk-jet interface* and indicated in Figure 4.1-1 by a dashed line.

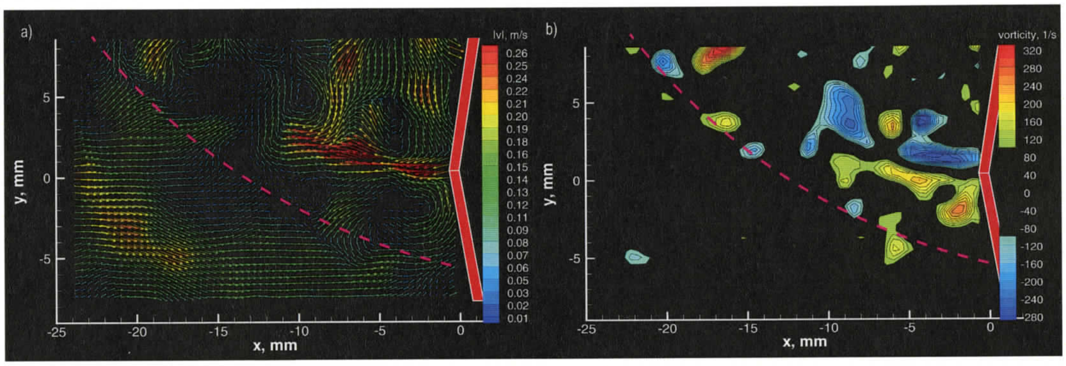

Figure 4.1-1 Patterns of instantaneous velocity (a) and out-of-plane vorticity (b) corresponding to the upward deflection of the central jet during the back flow phase (DAP CL-A)

High levels of vorticity are observed above the bulk-jet interface, where the central jet and its accompanying vortices are located. The out-of-plane vorticity plot of Figure 4.1-1 clearly shows counterclockwise rotating vortices being shed from the inner edge of the lower leaflet, while clockwise rotating vortices are shed from the inner edge of the upper leaflet. The highest levels of vorticity correspond to the shed vortices from the inner edges of the leaflets. Significant vorticity levels are observed up to 22 mm downstream of the valve.

In comparison, the region below the bulk-jet interface exhibits almost negligible levels of vorticity. The vast majority of the fluid located below the bulk-jet interface originates from the upstream bulk flow and therefore contains no large-scale vortical structures. Vortices shed from the outer edge of the lower leaflet are not observed in this particular case. It is suggested that they are located in the optically-inaccessible region along the bottom surface of the channel.

The subsequent characteristic phase of the flow oscillation cycle is referred to as the horizontal position of the central jet and is illustrated in Figure 4.1-2. During this phase, the central jet does not exhibit large-scale transverse deflections. Instead, the upstream bulk flow collides directly with the horizontal central jet and most of the upstream-moving fluid is forced out of the plane of view. Consequently, there is no clear bulk-jet interface, and the upstream bulk flow is split evenly by the central jet such that it is deflected in both the upward and downward transverse directions.

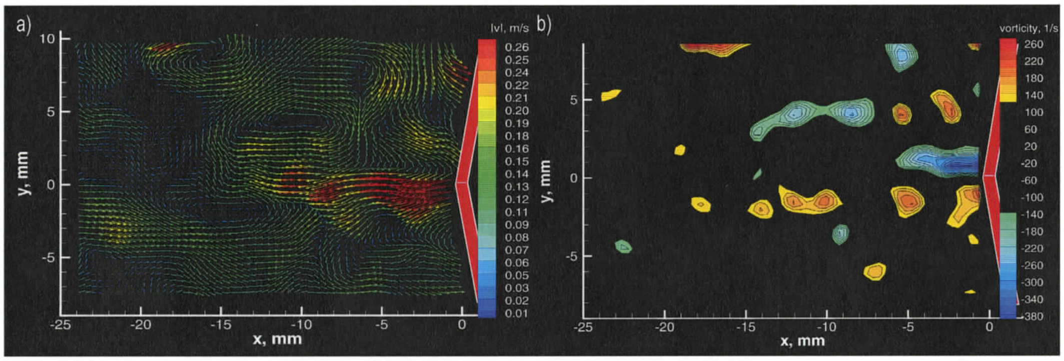

Figure 4.1-2 Patterns of instantaneous velocity (a) and out-of-plane vorticity (b) corresponding to the horizontal position of the central jet during the back flow phase (DAP CL-A)

The corresponding plot of the out-of-plane vorticity (Figure 4.1-2) shows significant levels of vorticity up to 20 mm downstream of the valve. Once again, the vortices shed from the outer edge of the lower leaflet are not observed due to the limited optical access along the bottom surface of the channel. However, two vortices with relatively high circulation levels are observed along the top edge of the out-of-plane vorticity plot. These vortices are shed from the outer edge of the top leaflet.

Patterns of instantaneous flow velocity and out-of-plane vorticity shown in Figure 4.1-3 correspond to the flow oscillation phase that is opposite to the upward central jet deflection of Figure 4.1-1. The central jet and the shed vortices from the inner edges of the leaflets are deflected downwards. Consequently, the upstream bulk flow is deflected upwards. High levels of vorticity are observed below the bulk-jet interface, which is indicated by a dashed line. In contrast, the only source of high circulation levels above the bulk-jet interface corresponds to the vortices that are shed from the outer edge of the top leaflet.

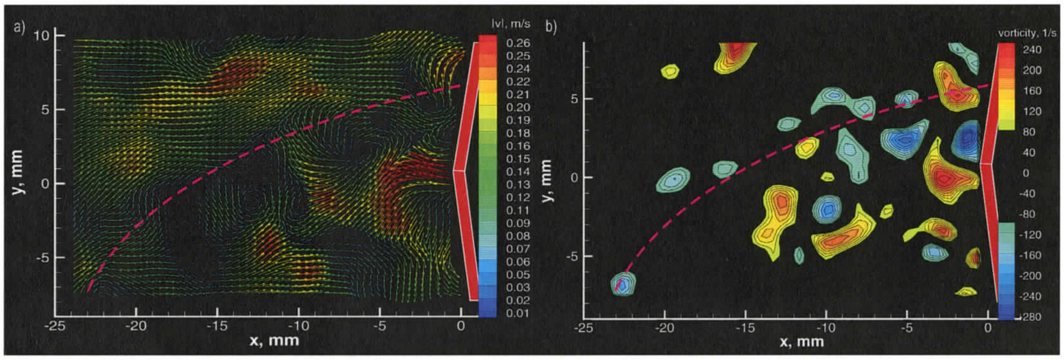

Figure 4.1-3 Patterns of instantaneous velocity (a) and out-of-plane vorticity (b) corresponding to the downward deflection of the central jet during the back flow phase (DAP CL-A)

It is evident that the frequency of the large-scale flow oscillation that is represented by the sequence of images in Figure 4.1-1 through Figure 4.1-3 is substantially lower than the frequency of the vortex shedding from the tips of the leaflets. In fact, at least three small-scale vortices are shed from the leaflet's edges during a typical large-scale oscillation cycle described above.

4.1.2 Time-averaged flow patterns

The images presented in this section are the result of ensemble-averaging of 1000 instantaneous images similar to those presented in the previous section.

The flow structure downstream of the fully closed valve is shown in the plot of time-averaged velocity and streamline patterns of Figure 4.1-4. The velocity field shows a high-velocity central jet, with a peak velocity of 0.26 m/s emerging between the two leaflets. The central jet collides with the low-speed bulk flow, which is moving in the upstream direction. This impingement causes the deflection of the upstream bulk flow towards the periphery of the channel. It should be noted that the vast majority of the upstream bulk flow deflects upwards while the central jet tilts slightly downwards.

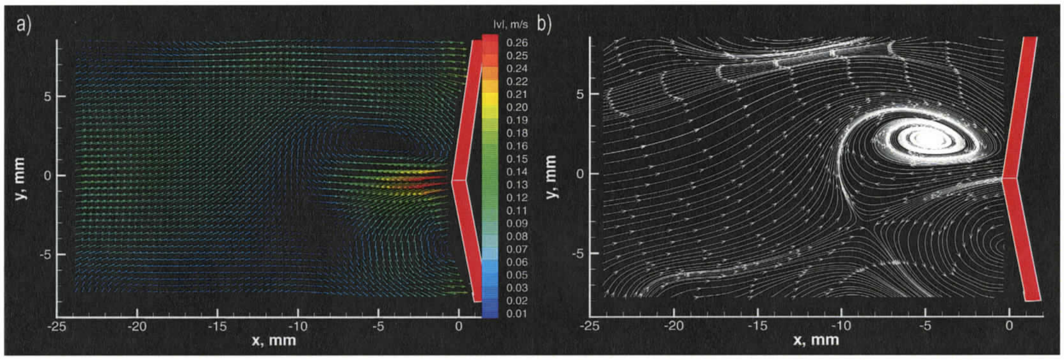

Figure 4.1-4 Time-averaged velocity (a) and streamline patterns (b) during the back flow phase (DAP CL-A)

The asymmetry of the flow structure is also illustrated by the plot of time-averaged streamline pattern of Figure 4.1-4. A saddle point is located 9 mm downstream of the valve at y = -4 mm. The location of the saddle point is consistent with the preference of the central jet to tilt toward the bottom surface of the channel. In addition, four large recirculation regions are observed. The two outermost recirculation regions (partially shown in the plot) correspond to the vortices that are shed from the outer edges of the leaflets. Similarly, the two inner recirculation regions correspond to the vortices that are shed from the inner edges of the leaflets.

Due to the unsteady nature of the inner pair of vortices, they are only advected, on average, approximately 5 mm downstream of the valve before the time-averaged vorticity associated with them is dissipated. On the other hand, the two outermost vortices advect, on average, approximately 12 mm downstream of the valve.

Figure 4.1-5 show patterns of velocity fluctuations in the wake of the valve in terms of root-mean-square of horizontal and vertical velocity components u_{rms} and v_{rms}. High levels of u_{rms} are associated with the unsteadiness of both the central jet and the vortices that are shed from the inner and outer edges of each leaflet. The peak levels of u_{rms} of 0.17 m/s occur at the locations where vortices are shed from the leaflets. Significant levels of u_{rms} are observed as far as 10 mm downstream of the valve. The peak values of v_{rms} of 0.14 m/s also occur at the location where vortices are shed from the leaflets.

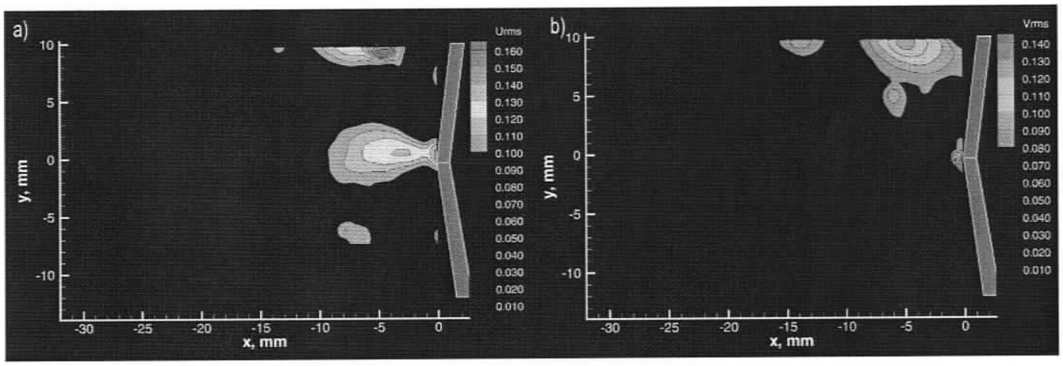

Figure 4.1-5 Root-mean-square of longitudinal (a) and radial (b) velocity fluctuations during the back flow phase (DAP CL-A)

The distribution of the velocity correlation <u′v′>, which corresponds to the dominant Reynolds shear stress component is shown in

Figure 4.1-6. Elevated values of <u'v'> are associated with the leakage flow that is observed between the two leaflets. The peak values of ±0.006 m^2/s^2 occur directly after the inner edges of the closed leaflets. The plot of Figure 4.1-6 provides an indication of the regions downstream of the closed valve where blood cells are subject to high stresses possibly contributing to the activation of platelets.

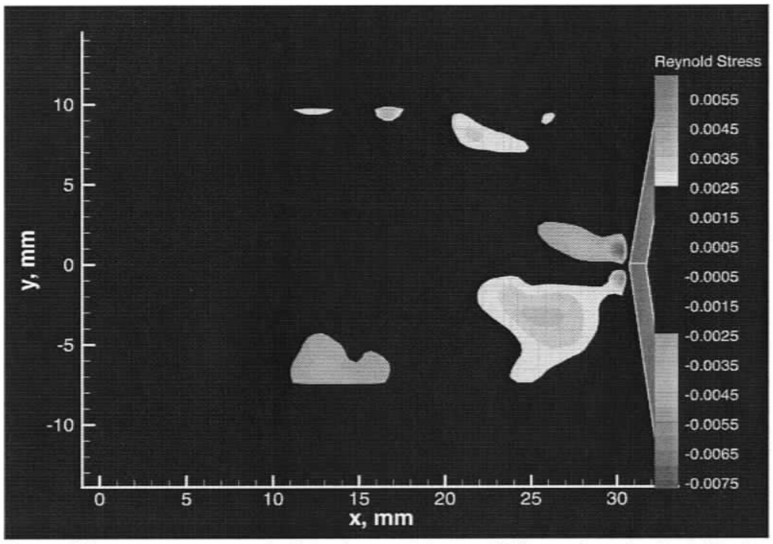

Figure 4.1-6. Reynolds stresses correlation downstream of the valve during the back flow phase (DAP CL-A)

4.2 Cross-stream Planes of View

The images in this section correspond to cross-stream cuts of the flow field. The bulk flow is directed out of the image plane. The valve's leaflets are not shown.

4.2.1 Instantaneous flow patterns

Figure 4.2-1 shows the instantaneous velocity field and the corresponding out-of-plane vorticity plot obtained at DAP CC-A, which is located 4 mm downstream of the valve's housing. Four high-velocity flow regions are observed. These regions, referred to here as the peripheral jets, corresponds to leakage through the valve hinges. Overall, the peripheral jets from the two bottom hinges are deflected upwards and away from the center of the channel. Similarly, the peripheral jets from the two top hinges are deflected downwards and away from the center of the channel.

Leakage flow through the bileaflet MHV is designed to occur primarily through the valve's hinges. This regurgitated flow prevents blood from stagnating in the hinges of the valve. Stagnant platelets can become activated and form blood clots around the valve's hinges, which could potentially disrupt the valve's performance or even cause thromboembolisms.

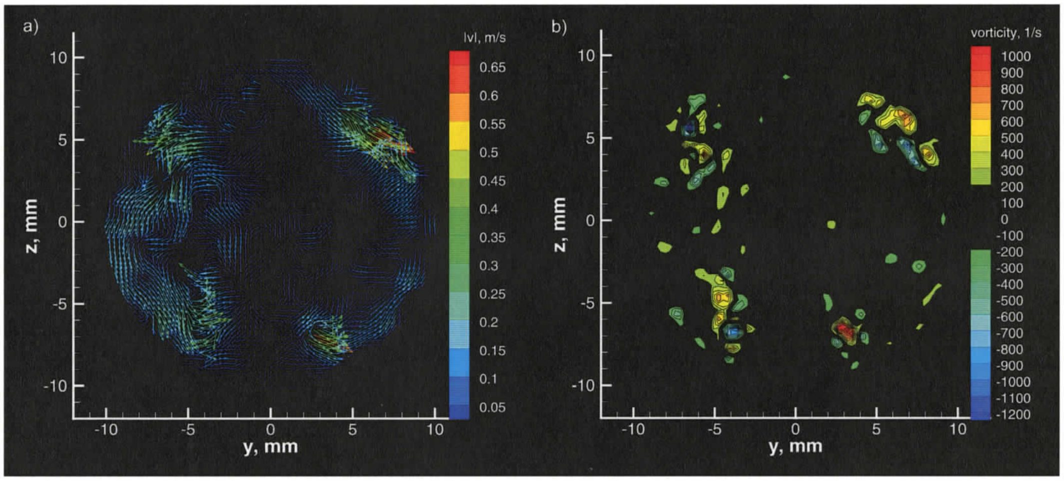

Figure 4.2-1 Instantaneous velocity field (a) and corresponding out-of-plane vorticity plot (b) for the case of the fully closed valve (DAP CC-A)

The plot of out-of-plane vorticity (Figure 4.2-1.b) shows peak circulation regions correspond to the location of the peripheral jets. Each of the four peripheral jets generates positive and negative vortices. All four of the regurgitant jets exhibit comparable velocity magnitudes, and generate similar circulation levels.

Figure 4.2-2 shows the instantaneous velocity field and the corresponding out-of-plane vorticity plot taken at DAP CC-B, 4 mm downstream of the valve. The bottom left and right peripheral jets have merged with the top left and right peripheral jets, respectively. The two pairs of merged jets are shown in Figure 4.2-2 by two high-velocity regions with radial velocity magnitudes similar to those of the peripheral jets, observed at DAP CC-A.

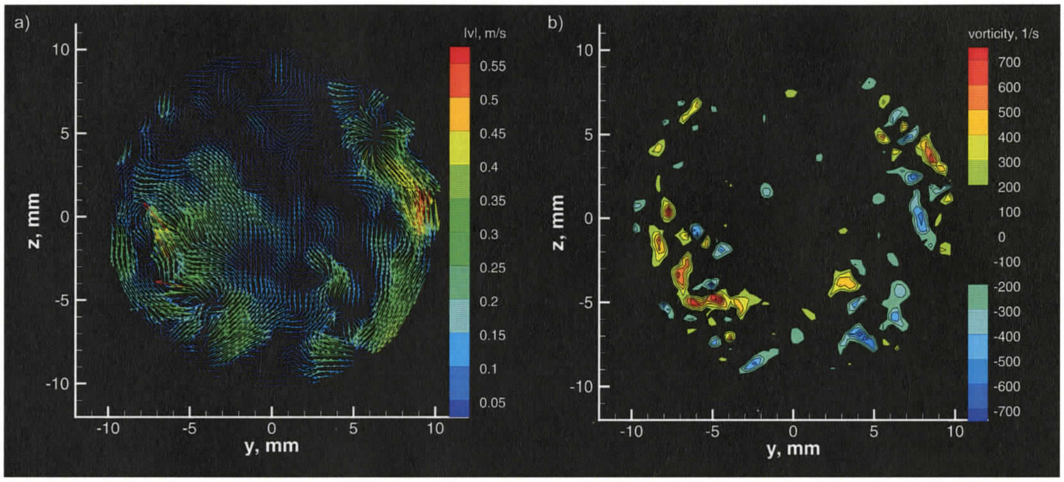

Figure 4.2-2 Instantaneous velocity field (a) and corresponding out-of-plane vorticity plot (b) for the case of the fully closed valve (DAP CC-B)

The location of peak vorticity levels, 4 mm downstream of the valve, correspond to the location of the merged jets. Both positive and negative vortices are observed.

Figure 4.2-3 shows the instantaneous velocity field and the corresponding out-of-plane vorticity plot for DAP CC-D. The left and right high-velocity regions have now merged to form one clockwise moving layer of fluid. Most of the fluid moves close to the periphery of the channel walls, with peak velocity magnitudes comparable to those observed in the previous two planes. The three dimensional flow structure represented by the cross-sectional plots of Figure 4.2-3 corresponds to a spiral flow moving along the x-axis.

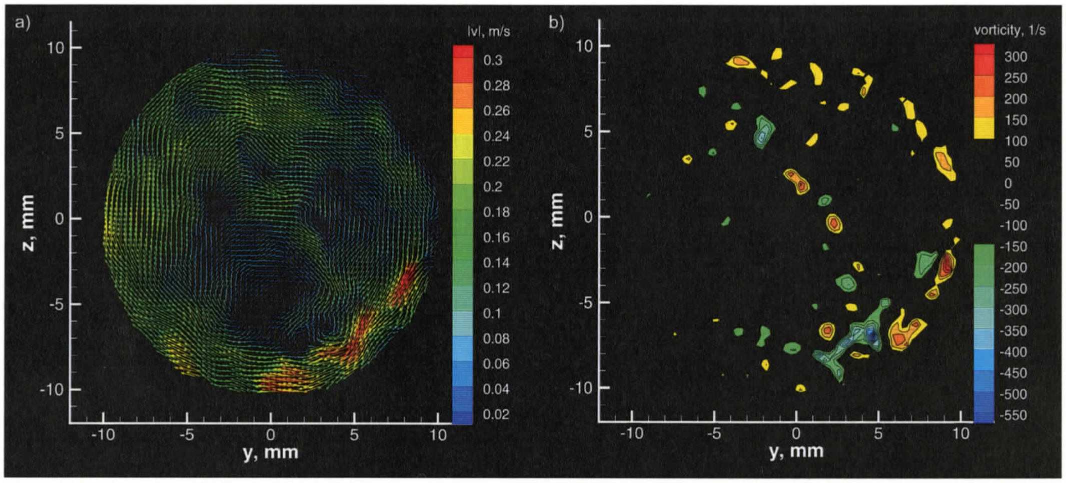

Figure 4.2-3 Instantaneous velocity field (a) and corresponding out-of-plane vorticity plot (b) for the case of the fully closed valve (DAP CC-D)

The levels of out-of-plane vorticity shown in Figure 4.2-3 are significantly lower than those observed in the previous two planes. The flow has reached a lower energy level 21 mm downstream of the valve represented in Figure 4.2-3 by an overall decrease of the vorticity levels.

4.2.2 Time-averaged flow patterns

The images presented in this section are a result of ensemble-averaging of 1000 instantaneous images similar to those presented in the previous section.

The time-averaged velocity field and its corresponding out-of-plane vorticity plot, obtained at DAP CC-A, are shown in Figure 4.2-4. High velocity regions are observed emerging from the top and bottom hinges of the fully closed valve. In all cases the high-velocity peripheral jets are deflected away from the channel walls and away from the valve's vertical axis of symmetry. In addition, a high-velocity flow emerges from the region between the two leaflets. This regurgitated flow does not travel parallel to the x-axis. Instead, it is deflected toward the left side of the valve, in agreement with the results of section 4.1.

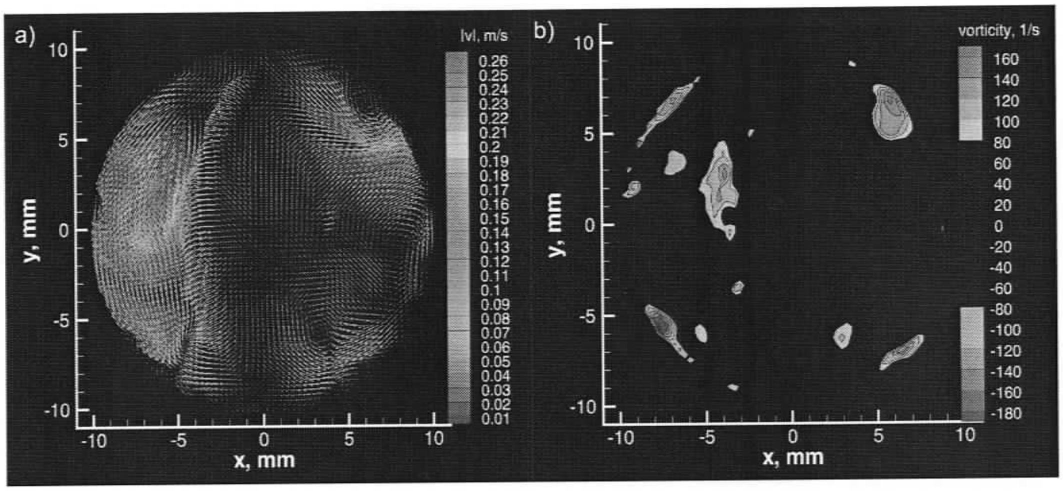

Figure 4.2-4 Time-average velocity (a) and out-of-plane vorticity (b) for the case of the fully closed valve (DAP CC-A)

The plot of the out-of-plane vorticity of Figure 4.2-4 shows five regions of high circulation. Four of these regions correspond to the peripheral jets, and one corresponds to the interaction between the top left peripheral jet and the regurgitant flow that originated from between the leaflets. Overall, the flow structure does not exhibit significant levels of out-of-plane vorticity.

The time-averaged velocity field and the corresponding out-of-plane vorticity plot obtained 14 mm downstream of the valve's housing, at DAP CC-C, are shown in Figure 4.2-5. Significant levels of vorticity are only observed close to the channel walls. The four regurgitant jets have merged with each other. The majority of the fluid is moving in the clockwise direction. In addition, a relatively large positive vortex forms close to the top left hinge of the valve.

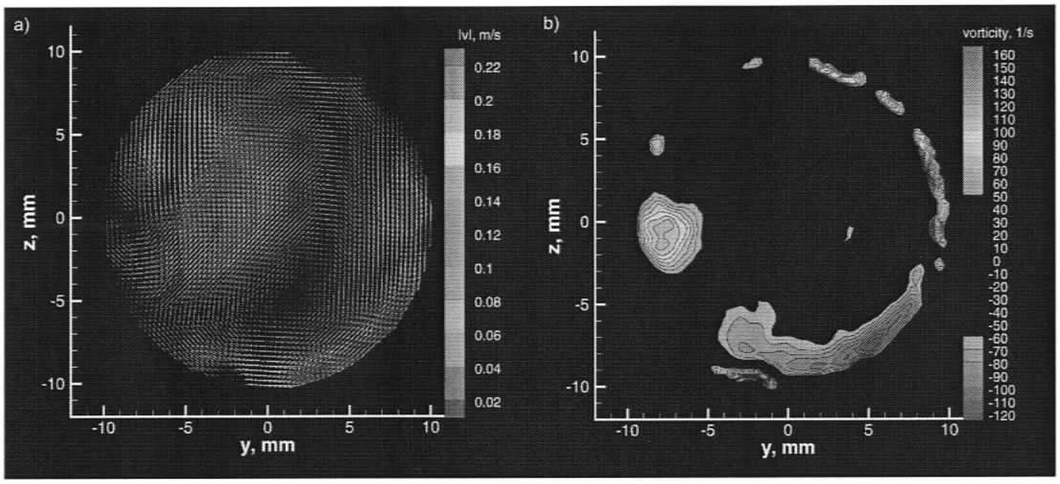

Figure 4.2-5 Time-average velocity (a) and out-of-plane vorticity (b) for the case of the fully closed valve (DAP CC-C)

Figure 4.2-6 shows the time-averaged velocity field and corresponding out-of-plane vorticity plot obtained at DAP CC-D. The region close to the channel walls exhibits relatively high velocity magnitudes, while low velocity regions are observed close to the center of the channel. The flow structure at DAP CC-D, 21 mm downstream of the valve, clearly represents an axial spiral flow.

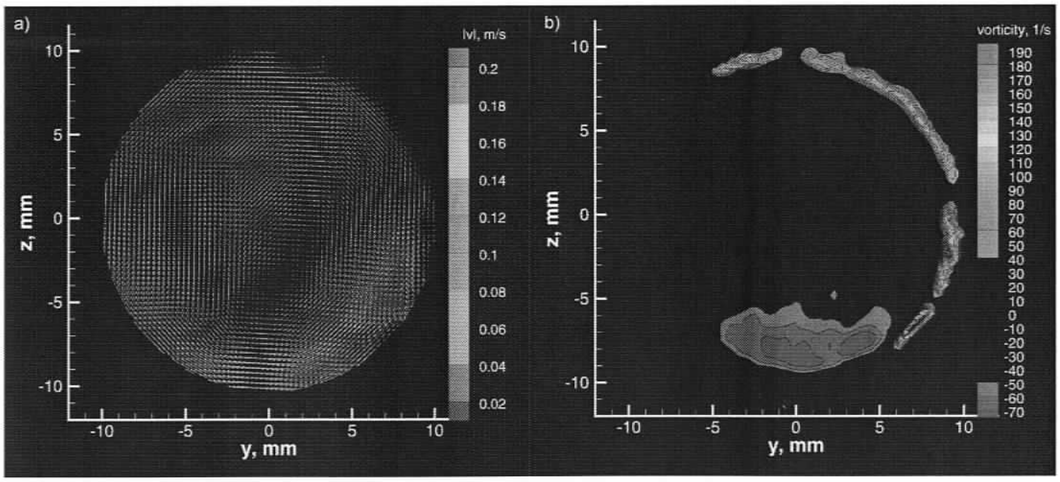

Figure 4.2-6 Time-average velocity (a) and out-of-plane vorticity (b) for the case of the fully closed valve (DAP CC-D)

The distribution of the velocity correlation <u′v′>, which corresponds to the dominant Reynolds shear stress component, obtained at DAPs CC-A through DAP CC-D, is shown in Figure 4.2-7. Peak Reynolds shear stress levels are an order of magnitude lower than those obtained at the longitudinal planes for the case of the fully open valve (DAP OL-A through DAP OL-E). Furthermore, in comparison to the longitudinal plane of the fully closed valve (DAP CL-A), the levels of <u′v′> are approximately 50% lower. Therefore, current results suggest the forward flow phase could potentially contribute more to the activation of platelets than the backward flow phase. Regions of high <u′v′> values correspond to the four peripheral jets and the regurgitant flow that originates from between the closed leaflets.

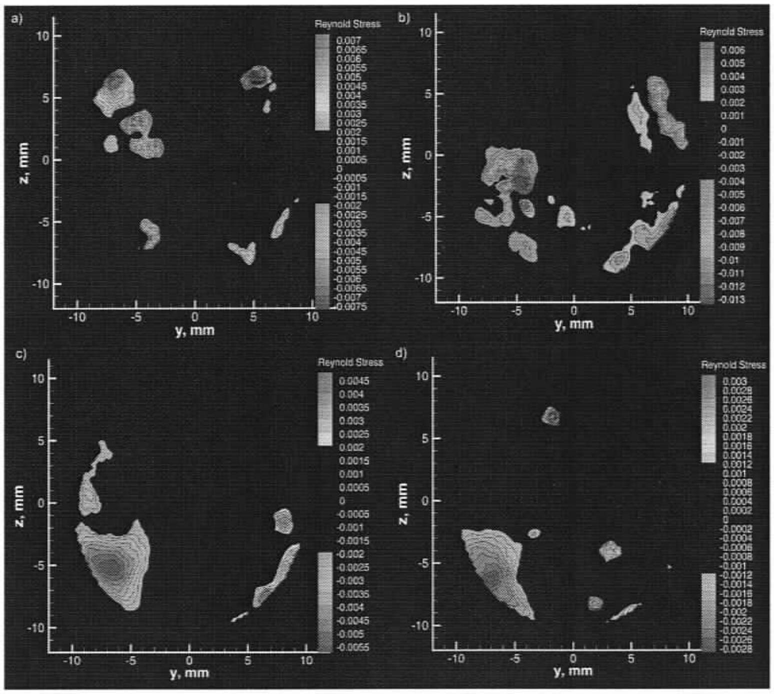

Figure 4.2-7 Reynolds shear stress correlation obtained at a) DAP CC-A, b) DAP CC-B, c) DAP CC-C, and d) DAP CC-D

Figure 4.2-8 shows patterns of velocity fluctuations, corresponding to DAP CC-A through DAP CC-D, in the wake of the valve in terms of root-mean-square of horizontal and vertical velocity components. Region of highly unstable flow are associated with the four peripheral jets, and their interaction downstream of the valve. Regions of high u_{rms} and v_{rms} levels provide an indication of the flow features that could possibly contribute to the activation of platelets, thus providing a background for future research.

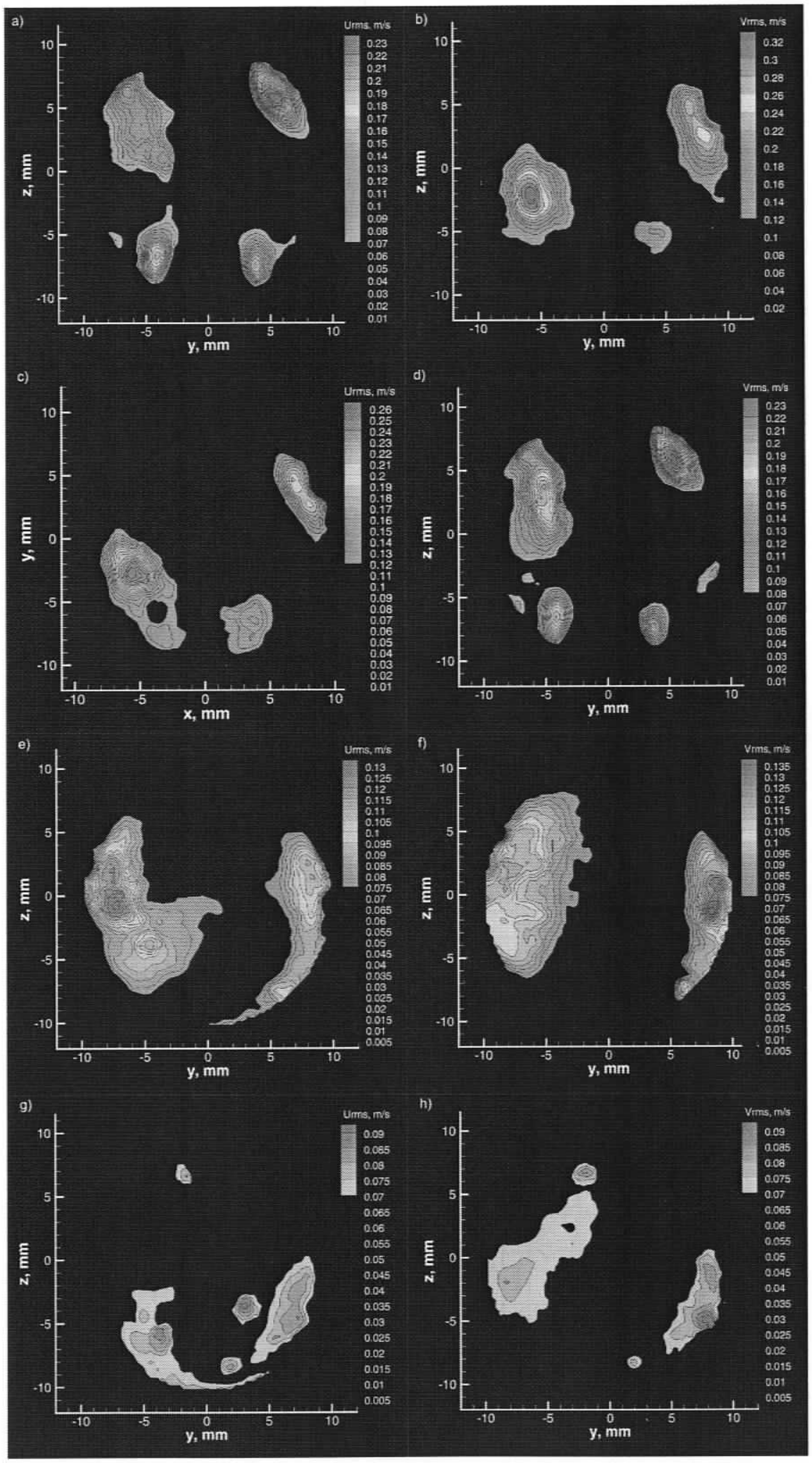

Figure 4.2-8 Root-mean-square of horizontal (a) and vertical (b) velocity components, obtained at DAP CC-A (a, b), DAP CC-B (a, b), DAP CC-C (a, b), DAP CC-D (a, b)

Chapter 5 Conclusions and Recommendations

Particle image velocimetry was used to investigate the flow structure downstream of a bileaflet mechanical heart valve (MHV) during peak systole (fully open valve) and peak diastole (fully closed valve). The data was obtained at a total of four sets of data acquisition planes (DAPs). Two sets of DAPs (longitudinal and cross-stream) were used for each of the two flow phases.

For the case of the fully open valve (peak systole), the overall flow structure consisted of four separated shear layers containing vortices shed from the leading and trailing edges of each leaflet. These shear layers define two wakes and a high-velocity jet-like region located between the two wakes. Two other high-velocity jet-like regions emerge from the side orifices of the fully open valve, located between the channel walls and each leaflet. Contrary to the traditional assumption of the dominant role of the outer shear layers, it was shown that the large-scale transverse oscillations of the inner shear layers dominate the near-wake of the valve. The large-scale flow oscillation corresponds to transverse undulations of the jet-like flow through the central opening of the valve and to flapping of the associated inner shear layers. These oscillations were characterized in terms of three representative flow regimes.

Furthermore, the flow directly downstream of the bileaflet MHV was found to be highly three-dimensional. Marked differences were found in the flow structure downstream of the MHV as the DAP moved along the vertical axis (z-axis). Predominantly, the central jet shifts position along the z-axis, causing an increase in the size of one wake and a reduction in size of the other. In general, the shift of the central jet causes a significant change in the unsteady flow structures present downstream of the valve. In addition, it was shown that the flow downstream of the fully open valve is not symmetric. Traditionally, it is assumed that the both leaflets are identical and their opening is symmetrical. However, current results suggest the asymmetry could potentially be a result of manufacturing tolerances large enough to affect the flow structure downstream of the fully open valve.

For the case of the fully closed valve (peak diastole), the bileaflet MHV was found to leak fluid at five different locations. The fluid leaks from the region between the two leaflets as well as from the gaps between the leaflets and the channel walls. However, the flow structure is dominated by the regurgitant flow that emerges from the valve's four hinges. The jets from all hinges interact with each other and eventually develop into an axial spiral flow, approximately 21 mm downstream of the valve.

Calculated Reynolds shear stresses were approximately 30%-50% higher for the fully open valve, in comparison to the back flow phase. However, limited temporal resolution did not allow for the calculation of pathlines. Therefore, it was not possible to accurately estimate the amount of cumulative stress experienced by a typical platelet. Nevertheless, current results help to identify potentially harmful regions of the flow structure for both the fully open and fully closed position of the bileaflet MHV.

At present, three parallel research paths for future investigations have been formulated. Naturally, it is necessary to model the opening and closing phases of the cardiac cycle. Therefore, a pulsatile flow pump is currently being designed and constructed. The pump will consist of a reciprocating piston driven by a fully programmable translation table.

Secondly, it is of primary importance to be able to measure the shear stresses at the surface of the leaflets. It would be expected that platelets activation would be greatest in the flow regions where their cumulative exposure to stress is highest. Therefore, surface shear stresses could potentially contribute to platelets' stress level such that they reach their activation threshold. Consequently, a transparent mock up of a bileaflet MHV has been developed (see Appendix C for a detail design of a transparent bilealflet MHV).

Finally, the possible causes for flow asymmetry downstream of the fully open bileaflet MHV will be investigated. Two rectangular plates will be positioned in a water channel, and the angle of attack of each plate will be controlled individually. In this way, the effect that the MHV leaflets' opening angle has on the near-wake flow structure can be assessed on a fundamental level.

The experimental study described here provided a background for these future studies.

Bibliography

[1] Johansen, P., 2004, Mechanical Heart Valve Cavitation, *Expert Rev Med Devices*, 1, 95-104.

[2] Yoganathan, A. P., He, Z., and Casey Jones, S., 2004, Fluid Mechanics of Heart Valves, *Annual Review of Biomedical Engineering*, 6, 331-362.

[3] Bellhouse, B., and Bellhouse, F., 1969, Fluid Mechanics of Model Normal and Stenosed Aortic Valves, *Circ Res*, 25, 693-704.

[4] Rossvoll, O., Samstad, S., Torp, H. G., Linker, D. T., Skjaerpe, T., Angelsen, B. A., and Hatle, L., 1991, The Velocity Distribution in the Aortic Anulus in Normal Subjects: A Quantitative Analysis of Two-Dimensional Doppler Flow Maps, *J Am Soc Echocardiogr*, 4, 367-378.

[5] Kilner, P. J., Yang, G. Z., Mohiaddin, R. H., Firmin, D. N., and Longmore, D. B., 1993, Helical and Retrograde Secondary Flow Patterns in the Aortic Arch Studied by Three-Directional Magnetic Resonance Velocity Mapping, *Circulation*, 88, 2235-2247.

[6] Roberts, W. C., 1976, Choosing a Substitute Cardiac Valve: Type, Size, Surgeon, *Am J Cardiol*, 38, 633-644.

[7] DeWall, R. A., Qasim, N., and Carr, L., 2000, Evolution of Mechanical Heart Valves, *Ann Thorac Surg*, 69, 1612-1621.

[8] Vesely, I., 2003, The Evolution of Bioprosthetic Heart Valve Design and Its Impact on Durability, *Cardiovasc Pathol*, 12, 277-286.

[9] Woo, Y.-R., Williams, F. P., and Yoganathan, A. P., 1983, In-Vitro Fluid Dynamic Characteristics of the Abiomed Trileaflet Heart Valve Prosthesis, 105, 338-345.

[10] Yin, W., Alemu, Y., Affeld, K., Jesty, J., and Bluestein, D., 2004, Flow-Induced Platelet Activation in Bileaflet and Monoleaflet Mechanical Heart Valves, *Ann Biomed Eng*, 32, 1058-1066.

[11] Snyder, T. A., Watach, M. J., Litwak, K. N., and Wagner, W. R., 2002, Platelet Activation, Aggregation, and Life Span in Calves Implanted with Axial Flow Ventricular Assist Devices, *Ann Thorac Surg*, 73, 1933-1938.

[12] Hellums, J. D., 1994, 1993 Whitaker Lecture: Biorheology in Thrombosis Research, *Ann Biomed Eng*, 22, 445-455.

[13] Bluestein, D., Yin, W., Affeld, K., and Jesty, J., 2004, Flow-Induced Platelet Activation in Mechanical Heart Valves, *J Heart Valve Dis*, 13, 501-508.

[14] Edmunds, L. H., Jr., McKinlay, S., Anderson, J. M., Callahan, T. H., Chesebro, J. H., Geiser, E. A., Makanani, D. M., McIntire, L. V., Meeker, W. Q., Naughton, G. K., Panza, J. A., Schoen, F. J., and Didisheim, P., 1997, Directions for Improvement of Substitute Heart Valves: National Heart, Lung, and Blood Institute's Working Group Report on Heart Valves, *J Biomed Mater Res*, 38, 263-266.

[15] Yoganathan, A. P., Chaux, A., Gray, R. J., Woo, Y. R., DeRobertis, M., Williams, F. P., and Matloff, J. M., 1984, Bileaflet, Tilting Disc and Porcine Aortic Valve Substitutes: In Vitro Hydrodynamic Characteristics, *J Am Coll Cardiol*, 3, 313-320.

[16] Scotten, L. N., and Walker, D. K., 2004, New Laboratory Technique Measures Projected Dynamics Area of Prosthetic Heart Valve, *Journal of Heart Valve Disease*, 13, 120-133.

[17] Marassi, M., Castellini, P., Pinotti, M., and Scalise, L., 2004, Cardiac Valve Prosthesis Flow Performances Measured by 2d and 3d-Stereo Particle Image Velocimetry, *Experiments in Fluids*, 36, 176-186.

[18] Kleine, P., Perthel, M., Nygaard, H., Hansen, S. B., Paulsen, P. K., Riis, C., and Laas, J., 1998, Medtronic Hall Versus St. Jude Medical Mechanical Aortic Valve: Downstream Turbulences with Respect to Rotation in Pigs, *J Heart Valve Dis*, 7, 548-555.

[19] Castellini, P., Pinotti, M., and Scalise, L., 2004, Particle Image Velocimetry for Flow Analysis in Longitudinal Planes across a Mechanical Artificial Heart Valve, *Artif Organs*, 28, 507-513.

[20] Zhao, J. B., and Yeo, J. H., 1999, Particle Image Velocimetry (Piv) Study on the Pulsatile Flow through Bileaflet Mechanical Aortic Heart Valves under Physiological Conditions, *American Society of Mechanical Engineers, Bioengineering Division (Publication) BED*, 42, 377-378.

[21] Brucker, C., Steinseifer, U., Schroder, W., and Reul, H., 2002, Unsteady Flow through a New Mechanical Heart Valve Prosthesis Analysed by Digital Particle Image Velocimetry, *Measurement Science and Technology*, 13, 1043-1049.

[22] Bluestein, D., Rambod, E., and Gharib, M., 2000, Vortex Shedding as a Mechanism for Free Emboli Formation in Mechanical Heart Valves, *Journal of Biomechanical Engineering, Transactions of the ASME*, 122, 125-134.

[23] Lamson, T. C., Rosenberg, G., Geselowitz, D. B., Deutsch, S., Stinebring, D. R., Frangos, J. A., and Tarbell, J. M., 1993, Relative Blood Damage in the Three Phases of a Prosthetic Heart Valve Flow Cycle, *Asaio J*, 39, M626-633.

[24] Manning, K. B., Kini, V., Fontaine, A. A., Deutsch, S., and Tarbell, J. M., 2003, Regurgitant Flow Field Characteristics of the St. Jude Bileaflet Mechanical Heart Valve under Physiologic Pulsatile Flow Using Particle Image Velocimetry, *Artificial Organs*, 27, 840-846.

[25] Meyer, R. S., Deutsch, S., Bachmann, C. B., and Tarbell, J. M., 2001, Laser Doppler Velocimetry and Flow Visualization Studies in the Regurgitant Leakage Flow Region of Three Mechanical Mitral&Nbsp;Valves, *Artificial Organs*, 25, 292-299.

[26] Lai, Y. G., Chandran, K. B., and Lemmon, J., 2002, A Numerical Simulation of Mechanical Heart Valve Closure Fluid Dynamics, *Journal of Biomechanics*, 35, 881-892.

[27] Hirt, F., Iten, R., and Ziada, S., Flow-Induced Oscillations of a Butterfly-Valve: Prediction of the Frequency Behaviour, *ASME*, Dallas, TX, USA, 53-2, 499-505.

[28] Cheng, R., Lai, Y. G., and Chandran, K. B., 2004, Three-Dimensional Fluid-Structure Interaction Simulation of Bileaflet Mechanical Heart Valve Flow Dynamics, *Annals of Biomedical Engineering*, 32, 1471-1483.

[29] Ellis, J. T., Healy, T. M., Fontaine, A. A., Saxena, R., and Yoganathan, A. P., 1996, Velocity Measurements and Flow Patterns within the Hinge Region of a Medtronic Parallel Bileaflet Mechanical Valve with Clear Housing, *J Heart Valve Dis*, 5, 591-599.

[30] Ellis, J. T., Travis, B. R., and Yoganathan, A. P., 2000, An in Vitro Study of the Hinge and near-Field Forward Flow Dynamics of the St. Jude Medical [Registered Trademark] Regent [Trademark] Bileaflet Mechanical Heart Valve, *Annals of Biomedical Engineering*, 28, 524-532.

[31] Adrian, R. J., 2005, Twenty Years of Particle Image Velocimetry, *Experiments in Fluids*, 39, 159-169.

[32] Adrian, R. J., 1984, Scattering Particle Characteristics and Their Effect on Pulsed Laser Measurements of Fluid Flow - Speckle Velocimetry Vs Particle Image Velocimetry, *Applied Optics*, 23, 1690.

[33] Adrian, R. J., 1991, Particle-Imaging Techniques for Experimental Fluid Mechanics, *Annual Review of Fluid Mechanics*, 23, 261-304.

[34] Westerweel, J., 1997, Fundamentals of Digital Particle Image Velocimetry, *Measurement Science & Technology*, 8, 1379-1392.

[35] Forliti, D. J., Strykowski, P. J., and Debatin, K., 2000, Bias and Precision Errors of Digital Particle Image Velocimetry, *Experiments in Fluids*, 28, 436-447.

[36] LaVision. (2002). *Flowmaster Manual*, LaVision, Gottingen.

[37] Martin, J. (2002). "Investigation of a U-Shaped Fuel Cell Flow Channel with Particle Image Velocimetry (Piv)," University of Victoria, Victoria.

Appendix A

The different calculated quantities used in the data analysis of this work are defined as follows:

- Vorticity (ω): in general defined as $\omega = \partial u / \partial i - \partial v / \partial j$. The first derivatives are approximated using a central difference approximation.
- Root-mean-square of the streamwise velocity component (u_{rms}):

$$u_{rms} = \left\{ \frac{1}{N} \sum_{n=1}^{N} \left[u_n(i,j) - < u(i,j) > \right]^2 \right\}^{1/2}, \tag{4}$$

- Root-mean-square of the radial velocity component (v_{rms}):

$$v_{rms} = \left\{ \frac{1}{N} \sum_{n=1}^{N} \left[v_n(i,j) - < v(i,j) > \right]^2 \right\}^{1/2}, \tag{5}$$

- Time-Averaged Reynolds Stress ($< u'v' >$):

$$< u'v' > = \frac{1}{N} \sum_{n=1}^{N} \left[u_n(i,j) - < u(i,j) > \right]\left[v_n(i,j) - < v(i,j) > \right], \tag{6}$$

Where u is the i-component of velocity, v is the j-component of velocity, and i and j are mutually perpendicular arbitrary directions. All these quantities, with the exception of the time-averaged Reynolds Stress, were computed using built-in functions available in the commercial software (Davis 6.2, Lavision, Germany) used here.

The Reynolds Stress was calculated using a Matlab code provided by Ting Yan at the University of Victoria. A copy of the code is shown below.

```
function rsdata(n)
n=60;
av=zeros(5742,2);
rs=zeros(5742,1);
  for k=1:n
    clear svel
    if k<=9
      identve=sprintf('velocity0000%g_0', k);
    elseif k<=99
      identve=sprintf('velocity000%g_0', k);
    else
      identve=sprintf('velocity00%g_0', k);
    end
    identrs=sprintf('rs%g',k);
    svel=sprintf('c:\\Documents and Settings\\Nauman\\Desktop\\MHV
7\\TecPlot\\W_O Background\\%s.txt',identve);
    velocity=textread(svel,'',-1,'headerlines',1);
    eval(['clear ', identve]);
    ylim=66;
    xlim=87;
    plim= xlim * ylim;
    av=av+velocity(:,3:4);
    eval([identrs, '=velocity(:,3:4);']);
  end
   av=av/n;
    for k=1:n
      identrs = sprintf('rs%g',k);
      eval([identrs, ' = ' ,identrs, '-av;']);
      uv=zeros(plim,1);
      for p=1:plim;
        eval(['uv(p,1) = ' ,identrs, '(p,1)*' ,identrs, '(p,2);']);
      end
      rs=rs+uv;
    end
    rs=rs/n;
    complete=[velocity rs];
    scom=sprintf('c:\\Documents and Settings\\Nauman\\Desktop\\MHV
    7\\TecPlot\\W_O Background\\reynolds _stress.txt');
    str1=sprintf('TITLE = "RS"');
    str2='VARIABLES = "x, mm"';
    str3='"y, mm"';
    str4='"u, m/s"';
    str5='"v, m/s"';
    str6='"Reynold Stress"';
    str7='ZONE T="ZONE 001"';
    str8='I=87, J=66, F=POINT';
```

```
    str_f=strvcat(str1,str2,str3,str4,str5,str6,str7,str8);
    fid=fopen(scom,'wt');
    for i=1:8
       fprintf(fid,'%s',str_f(i,:));fprintf(fid,'\n');
    end
    sz=size(complete);
    for i=1:sz(1)
       for j=1:5
          fprintf(fid,'%i\t',complete(i,j));
       end
       fprintf(fid,'\n');
    end
    fclose(fid);
return
```

Appendix B: Design of a Transparent MHV

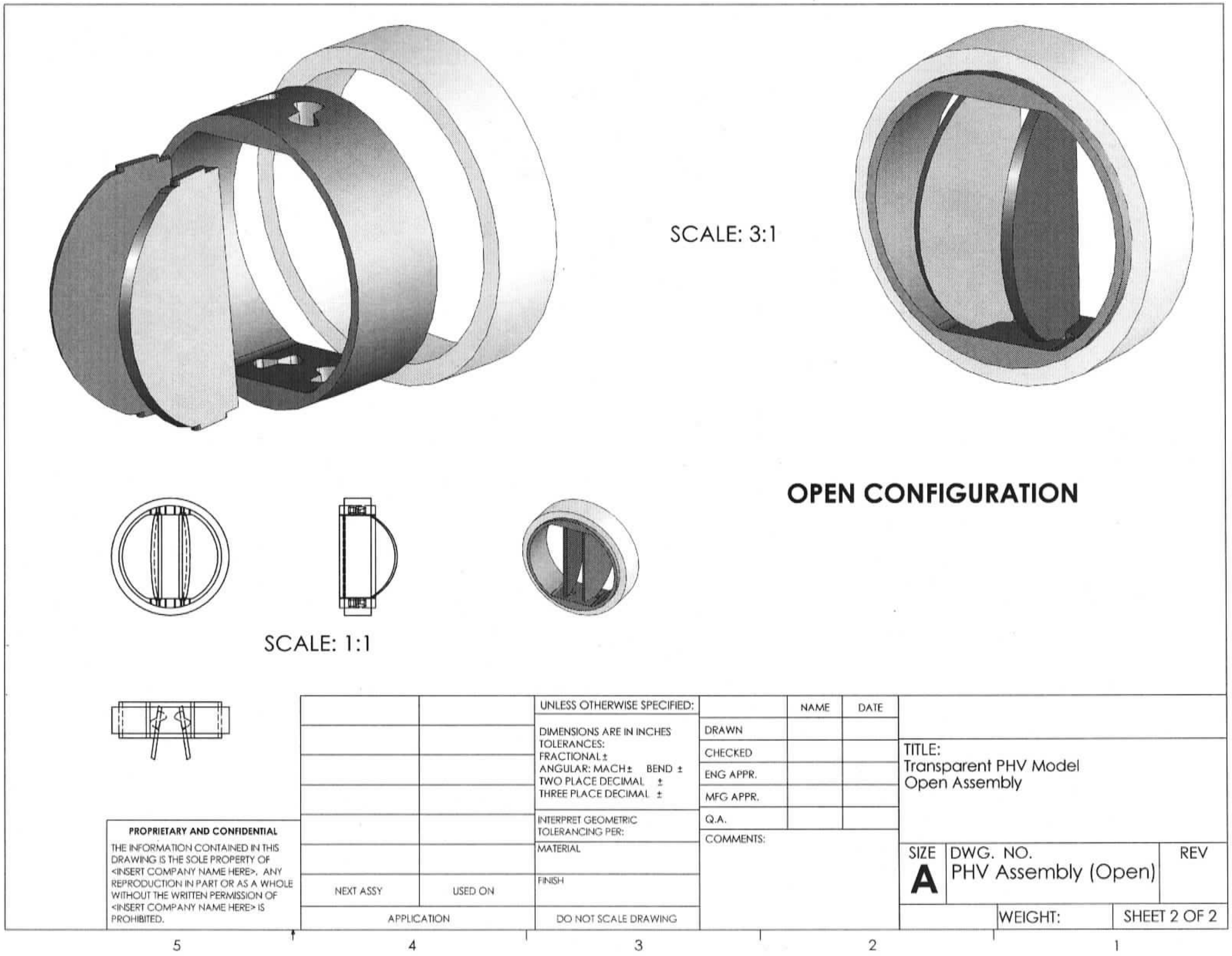

PROPRIETARY AND CONFIDENTIAL

THE INFORMATION CONTAINED IN THIS DRAWING IS THE SOLE PROPERTY OF <INSERT COMPANY NAME HERE>. ANY REPRODUCTION IN PART OR AS A WHOLE WITHOUT THE WRITTEN PERMISSION OF <INSERT COMPANY NAME HERE> IS PROHIBITED.

NEXT ASSY
USED ON
APPLICATION

UNLESS OTHERWISE SPECIFIED:
DIMENSIONS ARE IN INCHES
TOLERANCES:
FRACTIONAL ±
ANGULAR: MACH ± BEND ±
TWO PLACE DECIMAL ±
THREE PLACE DECIMAL ±
INTERPRET GEOMETRIC TOLERANCING PER:
MATERIAL
FINISH
DO NOT SCALE DRAWING

	NAME	DATE
DRAWN		
CHECKED		
ENG APPR.		
MFG APPR.		
Q.A.		

COMMENTS:

TITLE:
Transparent PHV Model
Open Assembly

SIZE A
DWG. NO.
PHV Assembly (Open)
REV
WEIGHT:
SHEET 2 OF 2

Note:
Both faces of the leaflet must be polished to 4 microinch finish.

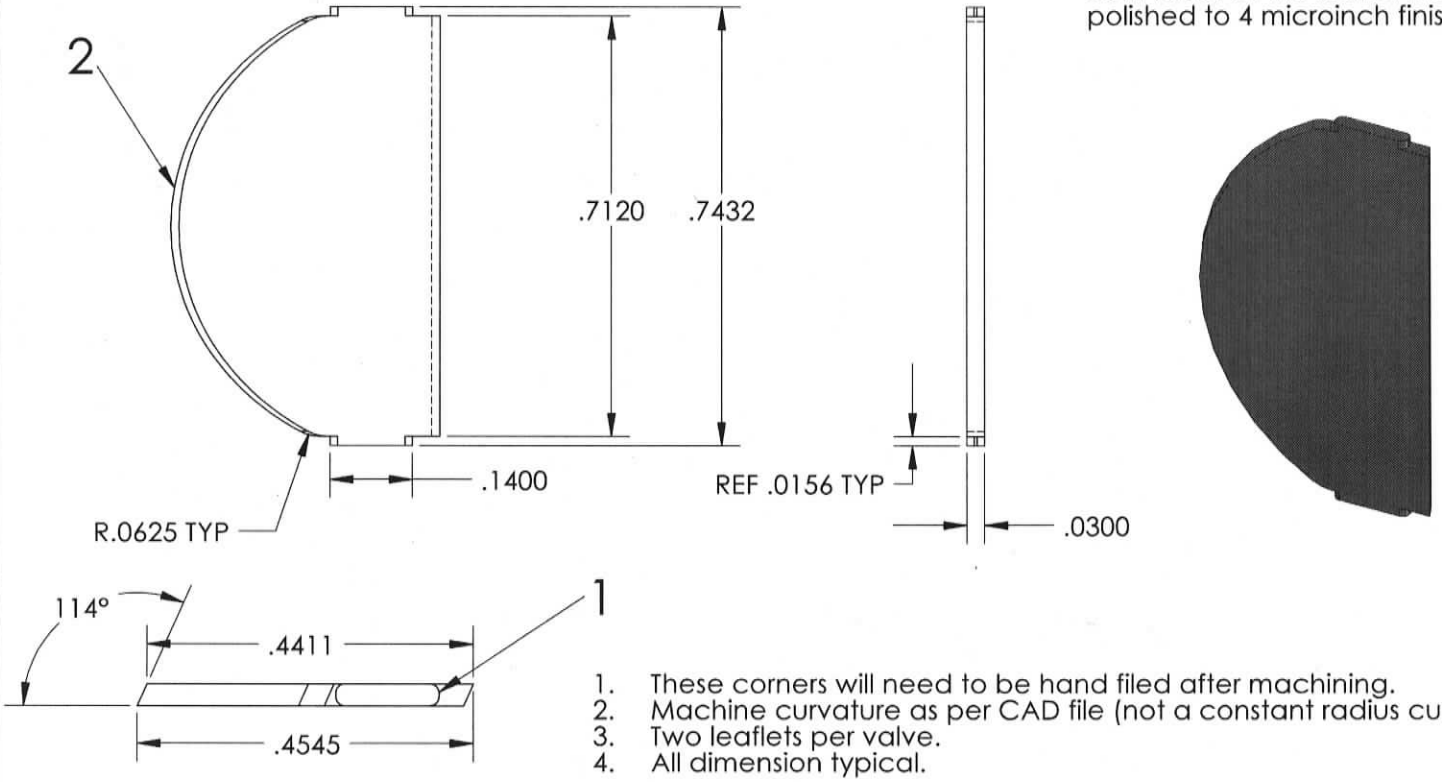

1. These corners will need to be hand filed after machining.
2. Machine curvature as per CAD file (not a constant radius curve).
3. Two leaflets per valve.
4. All dimension typical.

UNLESS OTHERWISE SPECIFIED:		NAME	DATE		
DIMENSIONS ARE IN INCHES TOLERANCES: FRACTIONAL± ANGULAR: MACH± BEND ± TWO PLACE DECIMAL ± THREE PLACE DECIMAL ±	DRAWN	Brett	08/16/05		
	CHECKED			TITLE: Transparent PHV Model Leaflet	
	ENG APPR.				
	MFG APPR.				
INTERPRET GEOMETRIC TOLERANCING PER:	Q.A.				
MATERIAL Optically Clear Polycarbonate	COMMENTS:			SIZE A	DWG. NO. Transparent Leaflet
FINISH 4 microinch					REV
DO NOT SCALE DRAWING				SCALE: 1:1 WEIGHT:	SHEET 1 OF 1

NEXT ASSY	USED ON
APPLICATION	

PROPRIETARY AND CONFIDENTIAL

THE INFORMATION CONTAINED IN THIS DRAWING IS THE SOLE PROPERTY OF THE UNIVERSITY OF VICTORIA. ANY REPRODUCTION IN PART OR AS A WHOLE WITHOUT THE WRITTEN PERMISSION OF THE UNIVERSITY OF VICTORIA IS PROHIBITED.

5 4 3 2 1

Note:
Both the inner and outer
ring surfaces must be polished
to optical grade 4 microinch finish.

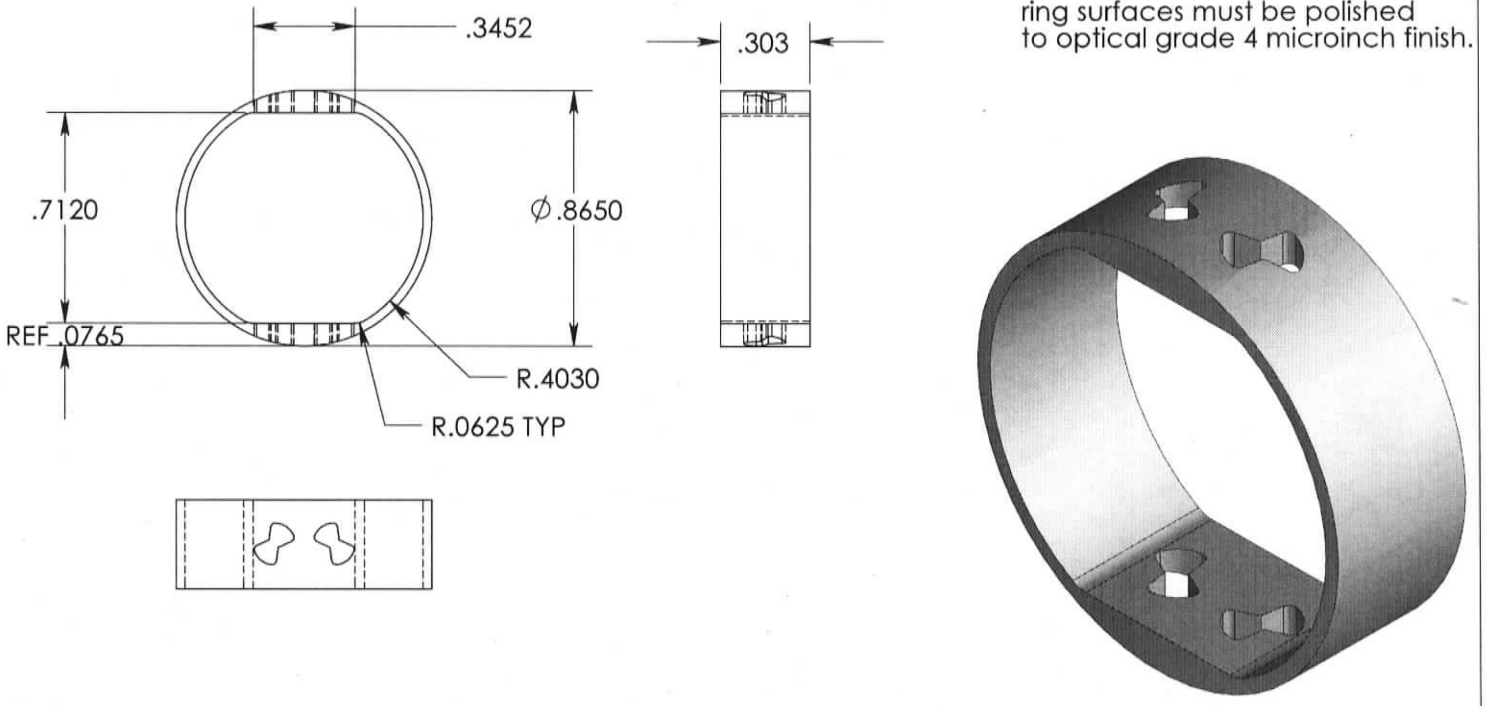

See sheet 2 for section and detail views.

UNLESS OTHERWISE SPECIFIED:		NAME	DATE	
DIMENSIONS ARE IN INCHES TOLERANCES: FRACTIONAL ± ANGULAR: MACH ± BEND ± TWO PLACE DECIMAL ± THREE PLACE DECIMAL ±	DRAWN	Brett	08/16/05	
	CHECKED			TITLE: Transparent PHV Model Inner Ring
	ENG APPR.			
	MFG APPR.			
INTERPRET GEOMETRIC TOLERANCING PER:	Q.A.			
MATERIAL Optically Clear Polycarbonate	COMMENTS:			SIZE A DWG. NO. Transparent Inner Ring REV
FINISH 4 microinch				
DO NOT SCALE DRAWING				SCALE: 2:1 WEIGHT: SHEET 1 OF 2

APPLICATION

PROPRIETARY AND CONFIDENTIAL

THE INFORMATION CONTAINED IN THIS DRAWING IS THE SOLE PROPERTY OF THE UNIVERSITY OF VICTORIA. ANY REPRODUCTION IN PART OR AS A WHOLE WITHOUT THE WRITTEN PERMISSION OF THE UNIVERSITY OF VICTORIA IS PROHIBITED.

5 4 3 2 1

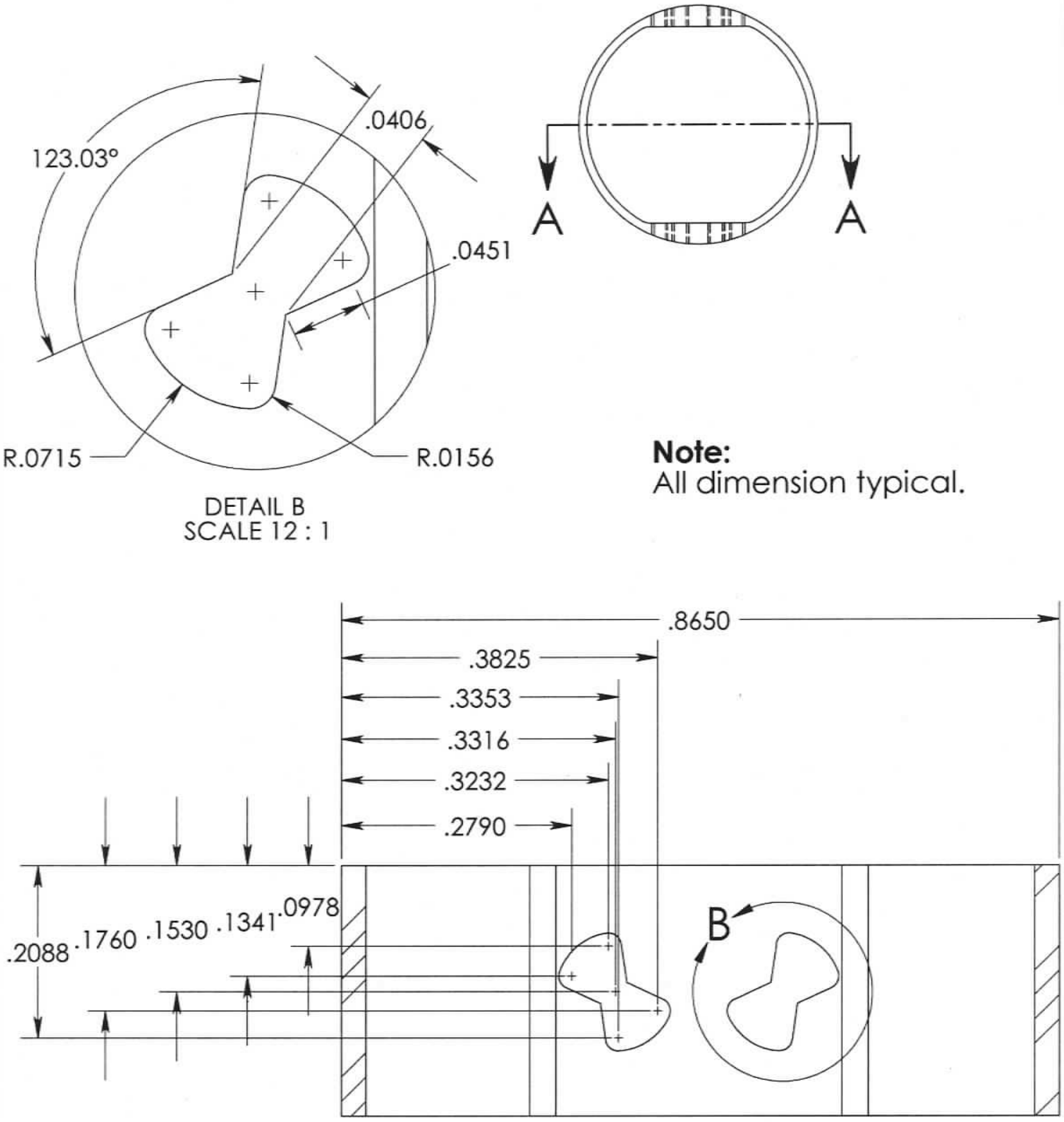

DETAIL B
SCALE 12 : 1

Note:
All dimension typical.

SECTION A-A
SCALE 6 : 1

DIMENSIONS ARE IN INCHES
TOLERANCES:
FRACTIONAL ±
ANGULAR: MACH ± BEND ±
TWO PLACE DECIMAL ±
THREE PLACE DECIMAL ±

	NAME	DATE
DRAWN	Brett	08/16/05
CHECKED		
ENG APPR.		
MFG APPR.		
Q.A.		

COMMENTS:

PROPRIETARY AND CONFIDENTIAL
THE INFORMATION CONTAINED IN THIS DRAWING IS THE SOLE PROPERTY OF THE UNIVERSITY FO VICTORIA. ANY REPRODUCTION IN PART OR AS A WHOLE WITHOUT THE WRITTEN PERMISSION OF THE UNIVERSITY FO VICTORIA IS PROHIBITED.

MATERIAL
ABS Polycarbonate

FINISH
4 microinch

NEXT ASSY | USED ON
APPLICATION

DO NOT SCALE DRAWING

SIZE A
DWG. NO. Transparent Inner Ring
REV.
SCALE:2:1
WEIGHT:
SHEET 2 OF 2

Note:
Both the inner and outer
ring surfaces must be polished
to optical grade 4 microinch finish.

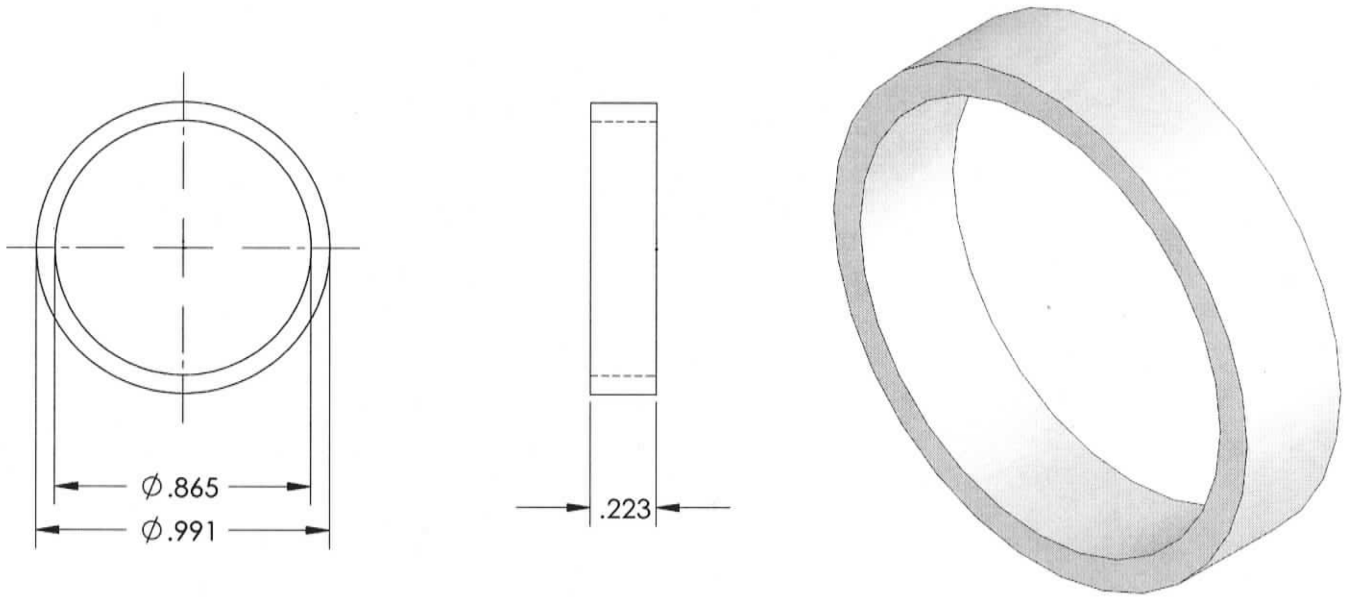

PROPRIETARY AND CONFIDENTIAL
THE INFORMATION CONTAINED IN THIS DRAWING IS THE SOLE PROPERTY OF THE UNIVERSITY OF VICTORIA. ANY REPRODUCTION IN PART OR AS A WHOLE WITHOUT THE WRITTEN PERMISSION OF THE UNIVERSITY OF VICTORIA IS PROHIBITED.

NEXT ASSY	USED ON
APPLICATION	

UNLESS OTHERWISE SPECIFIED:
DIMENSIONS ARE IN INCHES
TOLERANCES:
FRACTIONAL ±
ANGULAR: MACH ± BEND ±
TWO PLACE DECIMAL ±
THREE PLACE DECIMAL ±
INTERPRET GEOMETRIC TOLERANCING PER:
MATERIAL Optically Clear Polycarbonate
FINISH 4 microinch
DO NOT SCALE DRAWING

	NAME	DATE
DRAWN	Brett	08/15/05
CHECKED		
ENG APPR.		
MFG APPR.		
Q.A.		

COMMENTS:

TITLE:
Transparent PHV Model Inner Ring

SIZE A
DWG. NO. Transparent Outer Ring
REV

SCALE: 1:1 WEIGHT: SHEET 1 OF 1

5 4 3 2 1